Structures 55 (2023) 1354–1387

Contents lists available at ScienceDirect

Structures

journal homepage: www.elsevier.com/locate/structures

Development of hybrid rubber damper-restrainer (HRDR) system for structures under sever dynamic excitation

Ali Mahmoudi Mandani [a], Farzad Hejazi [b,*], Ali Nikkhoo [a]

[a] Department of Civil Engineering, University of Science and Culture, Tehran, Iran
[b] Faculty of Environment and Technology, The University of The West England, Bristol, United Kingdom

ARTICLE INFO

Keywords:
Vibration damper
Passive Control System
Finite Element Analysis
Rubber dampers
Earthquake

ABSTRACT

Nowadays, high damping rubber materials are extensively implementing in various types of structure to mitigate harmful effect of imposed vibration and dynamic force to the structure. Although, the rubbers exhibit noticeable damping in the shear action, however, de-bounding, shear rupture and delamination of rubber layers under cyclic loads, undermine the load-bearing capacity of the rubber dampers and increase their maintenance costs. Hence, the action of the rubbers is considerably high under applied compression to generate resistant force to restrain the deformation.

For this reason, in this research, a new hybrid rubber damper-restrainer (HRDR) system is proposed. The system comprises a high-damping rubber component designed to dissipate applied vibrations, along with a pair of hyper-elastic rubbers intended to restrain displacement. Therefore, the developed HRDR device is capable of dissipating vibrations while restraining large movements to prevent any damage and debounding of the rubber layers and also, protect the structure from excessive displacements.

To examine the performance of the proposed device, the numerical model of a HRDR was developed using the finite element simulation and subsequently, nonlinear dynamic analyses were conducted for the 6 storey prototype steel structure furnished with HRDR device. The findings revealed that the structure equipped with the HRDR device exhibited outstanding response against applied earthquake excitation which is proving high efficiency of HRDR device to diminish vibration effect on structure and prevent any excessive deformations. The HRDR device is applicable to any types of framed structures through installing via chevron brace system in steel structures or short wall in reinforced concrete structures. Furthermore, the developed HRDR device can be implemented in bridge structures, between the deck and pier of bridge to effectively dissipate vibrations and restrain the movement of the bridge span under traffic loads.

1. Introduction

The most common approach to classify the structural control systems is based on the functionality of the system indicating how the system works. In this classification, the control systems are categorized into four groups of passives, active, semi-active and hybrid [1]. Among these systems, the passive mechanism acts only after applying the external excitations and controls the structure's response. Thus, in the case of using such systems, the project would be economically more viable and a higher rate of reliability could be achieved. Fundamentally, the passive control systems dissipate a major portion of the input energy and in addition, enhance some of the characteristics of the structure such as strength, ductility etc [2]. In recent years, the passive control systems have been extensively developed, among which, the viscoelastic dampers (VEDs) could be addressed [3,4]. In 2016, Koblar and Boltezar evaluated the frequency-dependent damping ratio for the VEDs using experimental tests and numerical analyses [5]. Dong Hao studied the effect of pseudo-elastic materials that substantially depend on the deformation, frequency and temperature and subjected them to the static and harmonic loads [6]. In order to investigate this temperature and frequency-dependent behavior, a visco-elastic finite element model was proposed based on the models developed by Lion and Cardley (2004) and Hoofer and Lion (2009) [7,8]. Constitutive equations for the linear materials were prepared and then, extended for the elastic incompatible materials. Lastly, a process for simulating the parameters has been presented and some of the numerical results have been

* Corresponding author.
E-mail address: farzad.hejazi@uwe.ac.uk (F. Hejazi).

https://doi.org/10.1016/j.istruc.2023.06.106
Received 19 August 2022; Received in revised form 17 June 2023; Accepted 21 June 2023

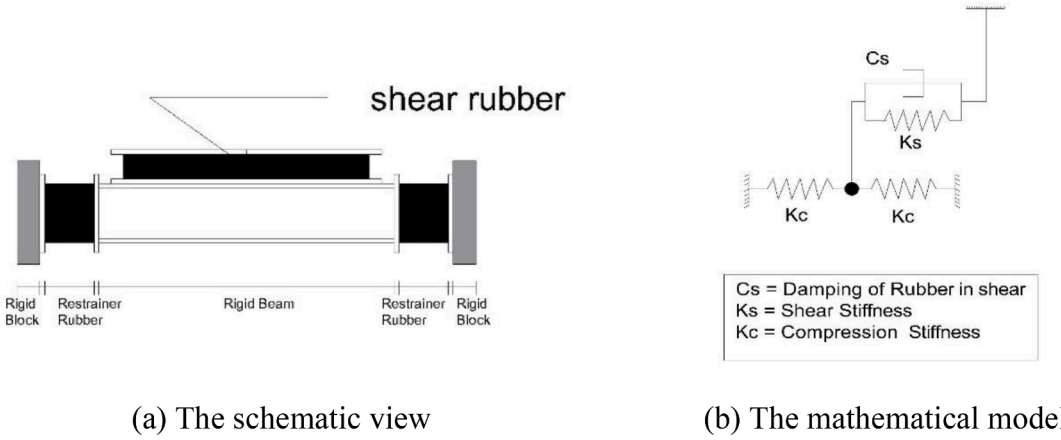

Fig. 1. The proposed Hybrid Rubber Damper-Restrainer (HRDR).

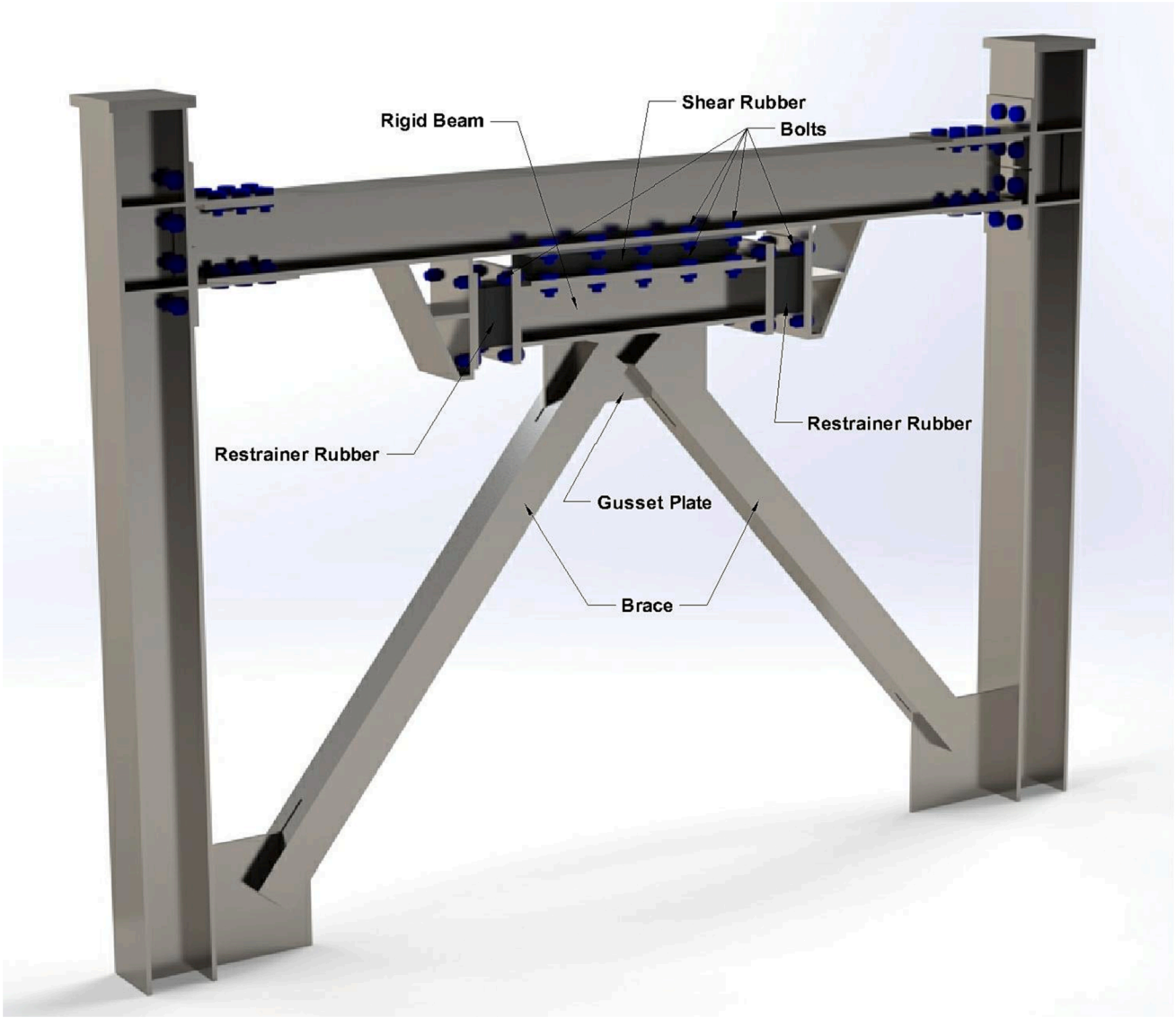

Fig. 2. The position of the HRDR damper in the frame with chevron braces.

delivered. In addition, experimental validation of the numerical models has been performed. In recent years, numerical tools such as finite element method have been broadly utilized for the purpose of optimization using the rubber dampers [9].

In 2015, Hejazi et al. studied the finite element model of a visco-elasto plastic damper to be used in the reinforced-concrete (RC)

frames. In this study, the rubber material implemented and numerically modelled as viscoelastic and viscoplastic material to dissipate vibration in medium and high deformation through elastic and plastic action of rubber respectively. The results of analyses on the structure with and without damper indicated that the dampers effectively dissipated the input energy [10]. In 2018, Bae and Karavasilis evaluated the seismic performance of the steel frames equipped with the visco-plastic dampers that are a combination of the visco-elastic and friction dampers [11]. Their major objective was to mitigate the storey shear forces without increasing the base shear. In this study, a moment-resisting steel frame was equipped with the visco-plastic dampers. For example, the maximum inter-storey drift under the MCE seismic hazard level was 1.2%. Moreover, a series of dynamic analyses were conducted on the frames equipped with the friction damper with varying sliding forces [12]. Promisingly, it was concluded that such dampers could markedly mitigate the base shear and limit the displacement and hence, prevent the structural collapse. Recently, research on developing the hybrid dampers to withstand the wind and earthquake loads has been carried out. A hybrid passive control damper (HPCD) consisting of high-damping rubber damper connected in series with a buckling-restrained brace (BRB), has been developed to dissipate the multilevel seismic energy. F. Hejazi and M. DaliliShoaei, A. Tousi & M. S. Jaafar examined the performance of the Viscous Wall Dampers using analytical models [3]. The results revealed that in the case of using such dampers, number of the plastic hinges in the beams and columns will be reduced. Furthermore, it was found that as the damping force increases, the shear forces and moments do not vary uniformly [13].

These investigations basically target the reduction of the seismic responses of structures against dynamic loads like earthquake, wind or blast. Based on review of the literature, it can be stated that there are crucial challenges regarding the rubber dampers as follows:

The most conventional vibration dissipation systems are base isolations which deflect or filters out the earthquake energy through a soft base component between the structure and the foundation. Such systems are suitable for short to medium height structures that usually have dominant modes in the high frequency range [14]. However, overturning moments and also application of base isolation in existing structure are the most challenging issue for these systems.

Performance of the viscous dampers is function of the load velocity, which limited their function only in high frequency excitations. Hence, the rubber which is considered as viscoelastic materials exhibits high shear resistant force when it experiences of deformation even in low-speed force as its function is not dependent on load frequency. Although damping action of rubber material increases in higher load frequencies, but its shear stiffness is not velocity dependent. However, the main drawback of rubber dampers is debounding and delamination of the rubber layers when frequently subjected to high deformations (100% to 300% elongation) such as cyclic load with high amplitude.

Although the rubber strength against applied axial load is very high and can be used as a movement restrainer in structures, but does not provide damping in compression or tension. Accordingly, use of the rubber dampers is limited due to debonding and delamination issues in long term excitation with high deformations. For this reason, in this study, a novel Hybrid Rubber Damper-Restrainer (HRDR) system is proposed by combination of rubber damping member and two rubber restrainer components installed in a beam connection to provide high load-bearing capacity restrainer system with desire damping capability which reduces the maintenance costs and enhance the effective life period of the damper device.

2. The proposed hybrid rubber damper restraint (HRDR) system

The rubber dampers have been widely used since 1970 s, and they have been used in the high-rise buildings to resist dynamic loads [15]. Analytical and experimental studies have shown that these dampers are reliable and sturdy, and evidence has convincingly supported their suitability to use in seismic designs. However, application of the rubber dampers in structures is limited due to rupture of bonding between rubber layers or between rubber and steel parts [16] which lead to the low shear strength of the device and high maintenance costs. In particular, this issue happens in the structures which are frequently subjected to dynamic loads such as parking or factory buildings and bridges [11]. For this reason, in this paper, HRDR System has been developed as illustrated in Fig. 1. As can be seen, the HRDR consists of:

i) A rigid short length steel beam with two steel plate at both ends.

ii) A high damping rubber layer component at the middle of the beam, which perform in shear and damp the applied vibration.

iii) Two hyper-elastic rubber components, positioned at the both end of rigid beam as restrainer parts which perform in compression to limit the applied vibration.

The developed hybrid system is installed within the frame structure with chevron bracing system as depicted in Fig. 2. Therefore, the device is positioned between chevron bracing and the top beam and it is connected to the top of chevron bracing connection plate using bolts and nuts. Similarly, high damping rubber installed at the middle of the rigid beam, is connected to the top beam of frame using bolt and nuts. In addition, the restrainer rubber parts are bolted to a pair of the rigid support arms welded to the top beam of frame as shown in Fig. 2.

As showed in setup details, the developed HRDR device is required to be installed through rigid bracing such as Chevron bracing or short rigid wall.

When the structure is excited by ground movement, the displacement is transferred to the HRDR device through the top beam of frame and the plate at the top of the chevron bracing. Then, the rigid beam starts to move and high damping rubber component deforms in shear. Moreover, one of the hyper-elastic rubbers which is in direction of movement, is compressed and the other hyper-elastic rubber is pulled. Through this mechanism, the high damping rubber component installed at the middle of the beam, restrains the applied displacement through its shear deformation and both hyper-elastic rubbers at the sides of beam. Since resistant force of the hyper-elastic rubber in compression is low in small deformations and exponentially increases in higher displacements, therefore, in low range of movement, the hyper-elastic rubbers do not function properly and then, the high damping rubber component effectively acts to dissipate the vibration.

However, by increasing movement, action of hyper-elastic rubber in compression highly increases by generating noticeable resistant force to limit the displacement and avoid damage to bounding of high damping rubber layers against excessive displacement.

The schematic view of the proposed HRDR device is presented in Fig. 1(b). Since high damping rubbers damp the vibration and also, generate resistant force against movement, they are modeled using a dashpot as well as a spring. However, since the hyper-elastic rubber only generates restrainer force without any damping during applied compression, it has to be modeled as a nonlinear spring only. The position of the proposed HRDR device in the frame structure with chevron bracing is depicted in Fig. 2.

3. The constitutive model for HRDR device

As demonstrated before, HRDR device is consisted of two components included of damping rubber and restrainer rubber which are acting as Hyper-elastic and Visco-elastic materials. Therefore, in order to simulate HRDE device through finite element method, the constitutive models for both of these materials are defined as explained in following:

3.1. Hyper-Elastic rubber material

The hyper-elastic materials are defining using two different analytical models which are derived based on the strain energy function [8]. One is the phenomenological models which treat the problem from the viewpoint of continuum mechanics and stress–strain behavior is

characterized without reference to the microscopic structure. The other one is physically motivated models which consider the material response from the viewpoint of microstructure.

In order to identify mechanical properties of rubber material, three following tests have been conducted:

i) Uniaxial Tension Test: This test is performed on the dumbbell specimen. There are two standards available for conducting this test, which are ASTM D412 standard [17] and ISO 37 standard [18]. Although both of these standards are defining same testing details and procedure, in this study ASTM D412 standard has been considered.

ii) Uniaxial Compression Set: This test has been demonstrated in ASTM D595 standard [19] and ISO7743 standard [20]. Testing setup and details of specimen for both mentioned standards are same.

iii) Simple Shear Test: The available standard for this test is ASTM D945 [21].

A brief detail about available hyper-elastic material models which exploited during this study is demonstrated as below:

i) Mooney-Rivlin model

The proposed analytical model is derived using two constants for material properties of the rubber related to compressibility and shear behavior of the rubber to make it absolutely appropriate for large stains in uniaxial elongation and shear deformation. But it cannot capture the upturn (S-curvature) of the force-extension relation in uniaxial test and the force-shear displacement relation in shear test. For a compressible rubber, this model is presented in the form of:

$$W = C_{10}(I_1 - 3) + C_{01}(I_2 - 3) + \frac{1}{D_1}(J_{el} - 1)^2 \quad (1)$$

where

C_{ij} = material constants that control the shear behavior and can be determined from uniaxial, biaxial and planar tests.

Di = material constant that control bulk compressibility and set to zero for fully incompressible rubber. It can be estimated from volumetric test. = ElasJ_{el}tic volume ratio.

ii) Neo-Hookean model

This model is a special case of Mooney-Rivlin form with $C_{01} = 0$ and can be used when material data is insufficient. It is simple to use and can make a good approximation at relatively small strains as shown in follow, but it is not able to capture the upturn of stress strain curve:

$$W = C_{i0}(I_1 - 3) + \frac{1}{D_1}(J_{el} - 1)^2 \quad (2)$$

where

C_{ij} = material constants that control the shear behavior and can be determined from uniaxial, biaxial and planar tests.

Di = material constant that control bulk compressibility and set to zero for fully incompressible rubber. It can be estimated from volumetric test. = ElasJ_{el}tic volume ratio.

iii) Full polynomial model

For isotropic and compressible rubber, polynomial model can be define as [22]:

$$W = \sum_{i,j=1}^{N} C_{ij}(I_1 - 3)^i (I_2 - 3)^j + \sum_{i=1}^{N} \frac{1}{D_i}(J_{el} - 1)^{2i} \quad (3)$$

where

C_{ij} = material constants that control the shear behavior and can be determined from uniaxial, biaxial and planar tests.

Di = material constant that control bulk compressibility and set to zero for fully incompressible rubber. It can be estimated from volumetric test.

J_{el} = Elastic volume ratio.

N = Number of terms in strain energy function.

iv) reduced polynomial model

This model does not include any dependency on I_2. The sensitivity of strain energy function to variation in I2 is generally much smaller than the sensitivity to variation in I_1. It appears that eliminating the terms containing I2 from strain energy function improves the ability of the models to predict the behavior of complex deformation states when limited test data is available. The Neo-Hookean form is first order reduced polynomial model.

v) Yeoh model

In 1993 [23], Yeoh proposed a phenomenological model for hyper-elastic material in the form of third-order polynomial based only on the first invariant. It can be used for the characterization of carbon-black filled rubber and can capture upturn of stress–strain curve. It has a good fit over a large strain range and can simulate various modes of deformation with limited data. This leads to reduce requirements for material testing to define rubber. The Yeoh model is also called the reduced polynomial model and for compressible rubber can be given as:

$$W = \sum_{i=1}^{3} C_{i0}(I_1 - 3)^i + \sum_{i=1}^{3} \frac{1}{D_i}(J_{el} - 1)^{2i} \quad (4)$$

where

C_{ij} = material constants that control the shear behavior and can be determined from uniaxial, biaxial and planar tests.

Di = material constant that control bulk compressibility and set to zero for fully incompressible rubber. It can be estimated from volumetric test.

J_{el} = Elastic volume ratio.

vi) Ogden model

This model is proposed in 1972 by Ogden [24]. This is also a phenomenological model and is based on principal stretches instead of invariants. The model is able to capture upturn (stiffening) of stress–strain curve and models rubber accurately for large ranges of deformation. This model should not use with limited number of material tests (e.g. just uniaxial tension). A good agreement has been observed between Ogden model and Treloar's experimental data for unfilled rubber for extensions up to 700%.

$$W = \sum_{i=1}^{N} \frac{2\mu_i}{\alpha_i^2}\left(\lambda_1^{\alpha_i} + \lambda_2^{\alpha_i} + \lambda_3^{\alpha_i} - 3\right) + \sum_{i=1}^{N} \frac{1}{D_i}(J_{el} - 1)^{2i} \quad (5)$$

where

λ_i is the deviatoric principal stretch and μ_i, α_i are temperature dependent material properties.

C_{ij} = material constants that control the shear behavior and can be determined from uniaxial, biaxial and planar tests.

Di = material constant that control bulk compressibility and set to zero for fully incompressible rubber. It can be estimated from volumetric test.

J_{el} = Elastic volume ratio.

N = Number of terms in strain energy function. Abaqus allows up-to 6 terms.

In this study, the Yeoh model is implemented to define the constitutive model for hyper-elastic rubber due to its ability to match experimental data points at small and large strain values.

3.2. The constitutive model for viscoelastic rubber material

In order to accurately describe the behavior of viscoelastic rubber materials, it is necessary to utilize an appropriate analytical model that takes into account the time-dependent effects. To define viscoelastic rubber materials, the appropriate analytical model with considering of the time effect on behaviour of viscoelastic rubber material is required to be implemented. The most important time effect is the relaxation phenomenon in which the material stiffness is reduced during the loading period. This is the well-known stress relaxation (or creep) effect that nearly all polymers exhibit when a certain load or deformation is applied. The most popular mathematical form of this behavior is given

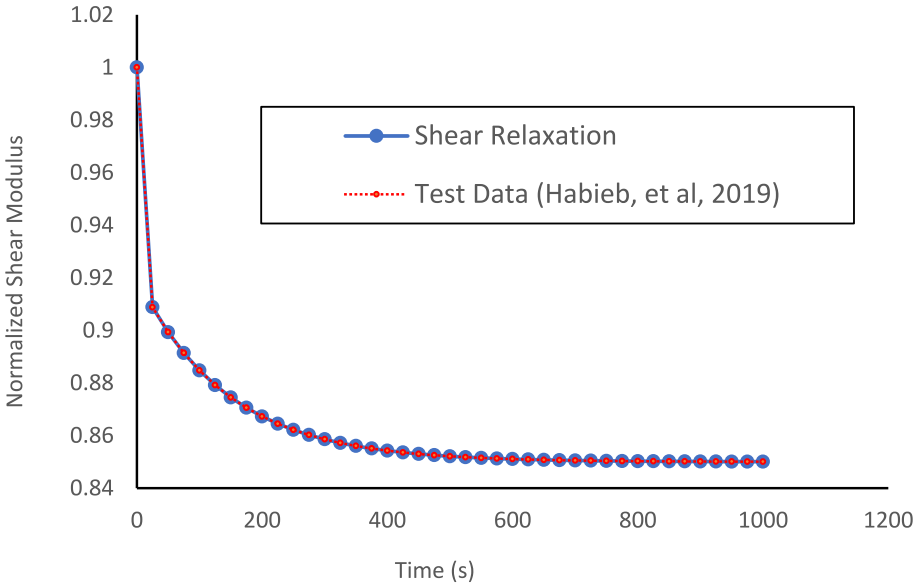

Fig. 3. Normalized stress-time history of relaxation tests (Habieb et al., 2019) and the shear relaxation corresponding to Prony model and its coefficients.

Table 1
Viscoelastic property constants for rubber materials (Prony series parameters).

	Prony series parameters			
Parameter	g_1	τ_1	g_2	τ_2
Obtained values	0.08	2.39E-5	‘0.07	142.83

Table 2
Chemical composition of rubber.

Natural Rubber (gms)	Carbon-Black (gms)	Stearic Acid (gms)	Zinc Oxide (gms)	MBT (gms)	Sulphur-80 (gms)
100	40	6	3	1	1

Table 3
Mechanical properties of rubber calculated by different tests.

Tensile Strength (MPa)	% Elongation	Shear Strength (MPa)	Shear Modulus (MPa)
12	610	4.6	0.36

by Prony series [25] as:

$$g_R(t) = \sum_{i=1}^{N} g_i^p (1 - e^{-\frac{t}{\tau_i}}) \quad (6)$$

$$k_R(t) = \sum_{i=1}^{N} k_i^p (1 - e^{-\frac{t}{\tau_i}}) \quad (7)$$

where g_i and k_i are a material constant and τ_i is the relaxation time and k_R is the bulk modulus. g_R is the dimensionless shear relaxation modulus defined as:

$$g_R(t) = \frac{G(t)}{G_0} \quad (8)$$

where G(t) and G_0 are the time dependent and the initial shear modulus, respectively. For hyper-elastic material models the relaxation Eq. (6) is normally applied to the constants that describe the energy function.

The normalized stress-time history of relaxation tests [26] and the shear relaxation corresponding to Prony model and its coefficients made through of present study have been showed in Fig. 3. Then using fitting curve, the Prony series parameters were calculated and listed in Table 1.

3.3. Properties of rubber material

Natural rubber reinforced by carbon-black was used for this research work as the chemical composition is given in Table 2. The nominal mechanical properties of the rubber as determined by various tests are given in Table 3.

3.4. Verification of finite element modeling for hyper-elastic rubber

Viscoelastic property, in conjunction with hyperelastic property of the rubber material, is also considered in this study. The viscoelastic property of the material provides a more accurate representation of the real world rubber behavior, and the finite element model should include consideration of this characteristic, especially for transient dynamic analysis.

This section describes the standard tests performed to use the stress–strain data for the rubber in the finite element modeling to evaluate the material constants for different hyper-elastic and visco-elastic models. Since the models are using a simple reversible stress–-strain input, the corresponding stress–strain function to the expected loading condition should be implemented.

An attempt has been made to observe the predefined behavior of a hyper-elastic or viscoelastic materials through the finite element modeling process. For this purpose, the material’s response has been calculated based on the experimental data using the strain energy potential. Subsequently, each type of coefficient for the strain energy or every type of instability in the material that is observed during the tests, must be considered.

3.4.1. Verification of hyper-elastic rubber model

The hyper elastic material curve fitting capability used to compare different hyper elastic material models with the test data. The validation of the hyper elastic models with experimental data has been done by many researcher by modeling the test specimens in different FE software. As highlighted before, an efficient hyper elastic material model should be independent from mode of deformation.

In ABAQUS software, the test data is specified as the nominal stress–strain data pairs for uniaxial, planar and biaxial tests to determine

Table 4
Coefficients of Mooney-Rivlin material model.

C10 (MPa)	C01(MPa)	D1	R^2
0.178	3.95E-03	0.110320166	0.9881

Table 5
Coefficients of Yeoh, Abaqus form, material model.

C10 (MPa)	C20 (MPa)	C30 (MPa)	D1	D2	D3	R^2
0.19	−1.9E-3	5.62E-05	0.1057	0	0	0.9962

Table 6
Coefficients of ogden, n = 3, material model.

Mu_I	Alpha_I	D_I	R^2
0.4451	–0.2241	1.824e–3	0.9896
3.2898	4.3753	4.596 e–5	
2.8917	–2.783	–7.334 e–7	

Table 7
Coefficients of Arruda-Boyce material model.

Mu	Mu_0	Lamda_M	D	R^2
0.4283	0.4462	3.9142	1.712 e–3	0.9902

Table 8
Coefficients of Neo-Hookean material model.

C10 (MPa)	D1	R^2
0.2587	1.5828e–3	0.9710

the shear constants C_{ij} and to determine the compressibility constants D_{ij}, pressure–volume ratio data which can be specified for the volumetric test data.

The C3D20RH elements were used for the rubber pads where "H" represents hybrid formulation. As the rubber is nearly incompressible, bulk modulus is much larger than shear modulus, FE solution will result in various errors with normal elements such as small change in displacements that causes extremely large changes in pressure, volume strain locking, etc. In order to overcome such issues, hybrid elements are used in which compression is treated as an independently interpolated solution variable that is coupled with displacement solution through constitutive theory.

For each stress–strain data pair, an equation for the stress is generated in terms of the strain invariants or stretches and the unknown hyper elastic constants. The test data, for different deformation modes, were specified and hyper elastic material models were evaluated to fit with the experimental data. The Yeoh model appeared to be the most suitable choice for predicting the behavior of the given rubber composition behavior because of its ability to match the experimental data points at small and large strain values. The coefficients of Mooney-Rivlin, Neo-Hookean, Yeoh model, Arruda-Boyce and Ogden models as calculated by FEM software, are given in Tables 4–8 with their average R2 values for all deformation modes.

3.4.2. Verification of viscoelastic rubber model

There are two types of simple shear tests available for verification of the viscoelastic rubber including the dual lap shear test and quad lap shear test.

In the dual lap shear test, two rubber specimens are bonded between the three steel plates. During the testing, two outside plates are fixed and middle plate is displaced by the machine and then shear occurs in the rubber specimen. The details about this test are referred to the ASTM D945 standard [21].

The same concept is used for the Quad lap shear test, but four rubber specimens are used instead of using two rubber specimens in the quad lap test. To validate the Yeoh model coefficients, the finite element analysis was performed to predict the force and extension for quad lap (simple shear) and biaxial test specimen using FEM software.

To get experimental data, quad lap specimen was tested by Majid Shahzada (2015) in which four rubber pads were sandwiched between the steel plates with adhesive. Thickness of the rubber specimen was considered significantly lower than its width and length in order to minimize the bending effects. For modeling in the quad lap test using the finite element method, quadratic hex elements with reduced integration (C3D20R) were used in order to reduce the mesh density without affecting solution accuracy. In the developed model for the test specimen, one end of the specimen was constrained i.e. Ux = Uy = Uz = 0, whereas the opposite end was subjected to a displacement in the tension direction i.e. Ux = 60 mm in few steps.

Fig. 4 shows FE simulation of the quad lap specimen and the stress result in the rubber pads is shown in Fig. 5. A comparison of the experimental results with FE simulation of the quad lap specimen has proved a good agreement for the load-extension data. Therefore, the considered viscoelastic model for the rubber has been accurately verified.

There are many researches reported in the literature for using of Yeoh model to simulate the rubber material under cyclic load and the results are well verified. The investigations results are indicated that between all available constitutive model for rubber materials, Yeoh model is exhibiting more accurate close behaviour for Hyper-elastic materials such as rubber under cyclic loads [8,22,27,28] and [29].

Although, as respected reviewer mentioned, since rubber performance is changing by load frequency, therefore, velocity depended FEM model is more appropriate to simulate rubber behaviour. Hence as frequency range for applied cyclic loads to the structure is not too wide, therefore, Yeoh model for the considered range of load frequencies is leading to results with acceptable accuracy in comparison to experimental test outputs. By changing the load frequency, the rubber behaviour which simulated using Yeoh model is changing as well which

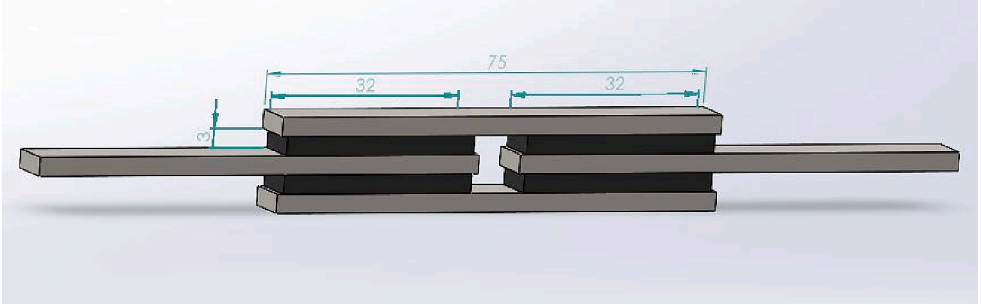

Fig. 4. Quad Lap Shear Test.

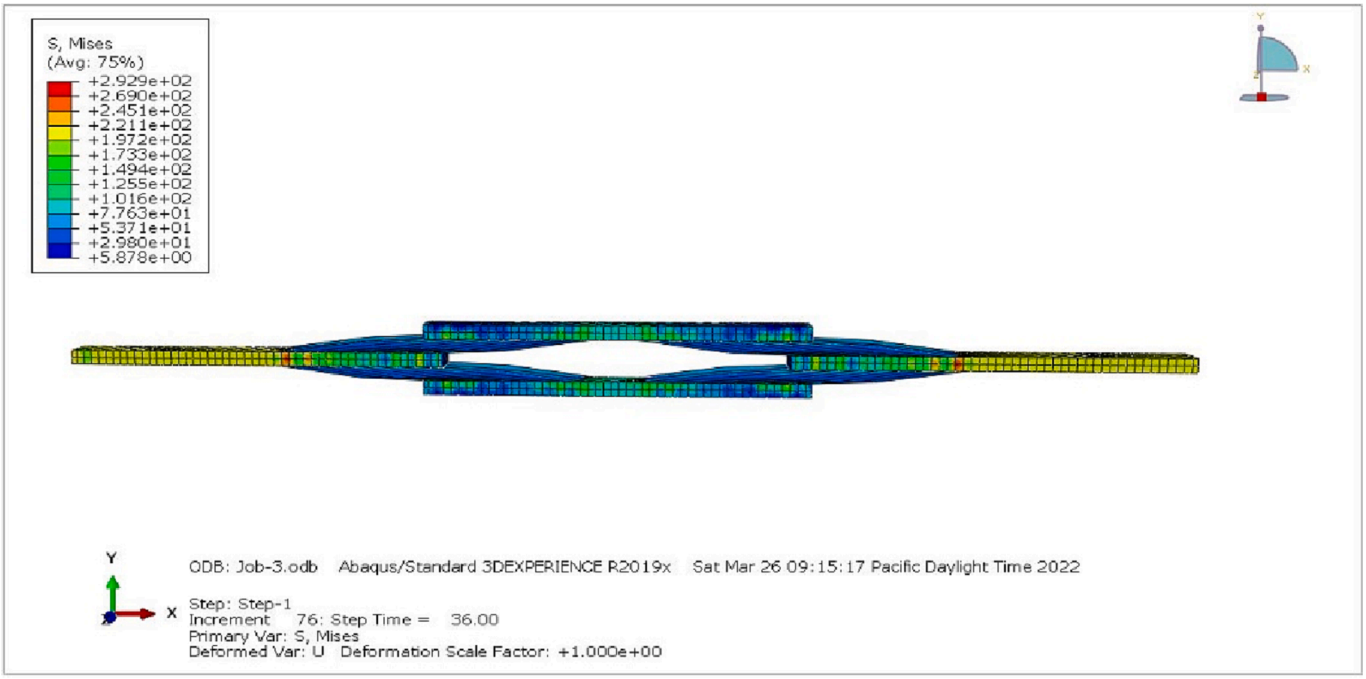

Fig. 5. FE simulation of quad lap specimen.

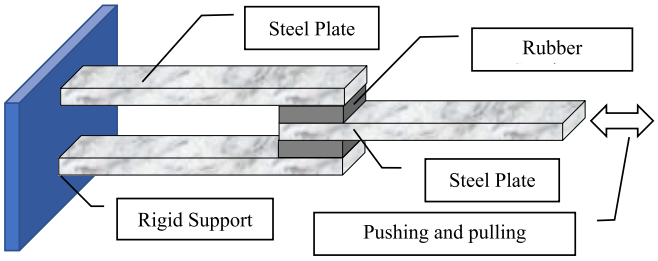

(a) Test setup for rubber testing under cyclic load

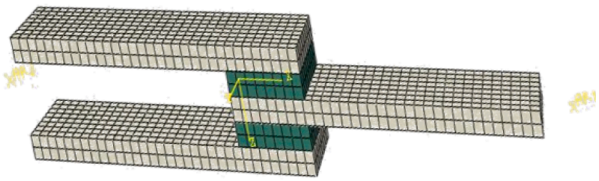

(b) Finite Element Model of rubber testing

Fig. 6. Configuration of rubber testing setup and its finite element simulation.

is indicating that the considered constitutive model is accommodating various force frequencies to reflect the corresponding performance of the rubber.

In this study also, behaviour of the rubber material under cyclic load also has been verified using the experimental test result of rubber specimen [28] which has been demonstrated in the next section:

3.5. Verification of rubber material simulation under cyclic load

As mentioned before, an attempt has been made in this study to verify the behaviour of high damping rubber material which defined using Yeoh model for finite element analysis under cyclic load. For this purpose, the experimental test results for the rubber material under cyclic load which conducted by Chen et al. (2019) [28] has been implemented to validate finite element model in this study. The test setup for rubber specimens has been showed in Fig. 6(a). As it can be seen in this figure, two rubber specimens with dimensions of 25 mm × 25 mm and 6 mm thickness are located within three steel plates with 100 mm length, 25 mm width and 6 mm thickness. The rubbers are bounded to the end part of steel plates through vulcanization and cyclic movement with amplitude of 12 mm has been applied to another end of middle steel plate to have deformation corresponding to 200% strain of rubber thickness. The end part of two other steel plates fixed using rigid support. The developed finite element model for this test is shown in Fig. 6(b).

The eight-node linear hexahedron reduced integration (C3D8R) elements is used for modeling of the steel plate connections.

The generalized Maxwell model is implemented for the constitutive model of the viscoelastic materials which consists of the hyperelastic constitutive model and the viscoelastic constitutive model. Among the demonstrated constitutive models, the Mooney–Rivlin model and the Yeoh model are applied for verification of constitutive model of high damping rubber in this section due to their high accuracy.

The amplitude correlation of the generalized Maxwell model needs to be considered by manual modifying the parameters of the constitutive model (equation (1) and (4)) for viscoelastic material under different strain conditions as showed in Table 9 [28]. It is assumed that the rubber

Table 9
Parameters to define High damping rubber [28].

Constitutive model	Applicability (γ:strain amplitude)	Fitting parameters			
		C10	C01	C20	C30
Mooney–Rivlin	20%≤ γ ≤ 150%	0.498932	0.034983	\mathord{-} -–0.00499	\mathord{-} \mathord{-} 0.00602
Yeoh	γ > 150%	0.50102	\mathord{-} \mathord{-}		

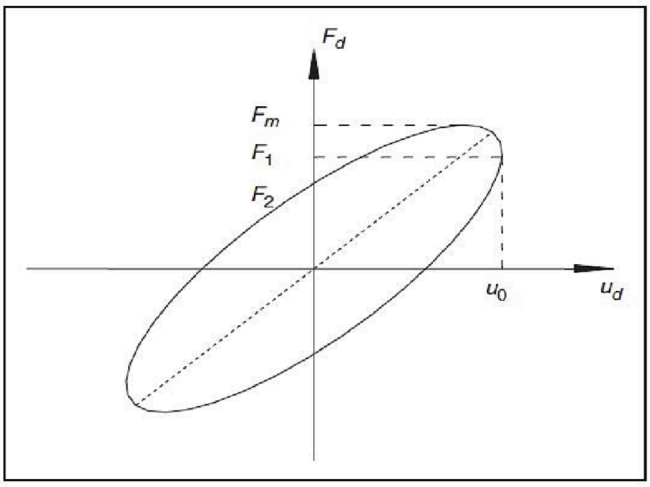

Fig. 7. Force-displacement hysteresis curve.

is an incompressible and isotropic material with the Poisson's ratio μ=0.5 and coefficient $D_i = 0$.

The simulation results are in good agreement with analysis test results corresponding to Yeoh function, which validates the accuracy of the implemented constitutive models for the rubber behaviour under cyclic loads. According to Chen et al. (2019) [28], the same results have been obtained for rubber deformation corresponding to 100% and 300% strain of rubber thickness. Therefore, the Yeoh model is applicable for any deformations up to 300% and above. Since the loads are applied with different frequencies and velocities for various deformations and results are still validated, therefore, it is concluded that the Yeoh mode is well fitted for rubber modeling under various load frequencies and speeds.

In another research, accuracy of various constitutive models for High Damping Rubber Material included of Mooney–Rivlin, Neo-Hookean, Van der Waals, Arruda–Boyce, Ogden (N = 3), Yeoh and Polynomial (N = 2) under cyclic loads with deformation corresponding to 100%, 200% and 300% strain for rubber thickness have been studied through experimental test results. This investigation has been concluded that Yeoh model is exhibiting the best accurate results for High Damping Rubber subjected to cyclic loads among all other considered constitutive models. After Yeoh model, the results corresponding to Arruda–Boyce, and Ogden (N = 3) functions have showed the next two more accurate responses with less than 10% error. It is highlighted that these analysis and test have been conducted with various load frequencies and load speed and results of simulations was within acceptable range of accuracy.

Therefore, based on abovementioned investigations conducted in this research and also by other researchers, the Yeoh constitutive model is considered and used in this study as the most accurate model to simulate high damping rubber materials under cyclic load with various range of amplitudes.

4. Evaluation performance of HRDR

After developing and verifying finite element model for the proposed HRDR device, an attempt has been made to evaluate its performance by applying cyclic load with various frequency and strains to investigate hysteresis response of device.

When VE dampers are incorporated in structures, the control forces generated by VE dampers.

is calculated using:

$$F_d = C_d\dot{\Delta} + K_d\Delta \tag{9}$$

where F_d is the forces produced by HRDR dampers, Δ and $\dot{\Delta}$ are the applied displacements and velocities to HRDR dampers, C_d and K_d are the equivalent damping and stiffness which can be determined through:

$$K_d = \frac{G_1 A_v}{h_v} \tag{10}$$

$$C_d = \frac{G_1 \eta A_v}{\omega h_v} \tag{11}$$

$$\eta = \frac{G_2}{G_1} \tag{12}$$

where η is the loss factor, G_1 and G_2 are the storage modulus and the loss modulus for the HRDR material in dampers, A_v and h_v are the area and thickness of the shear layer of HRDR dampers, ω is the excitation frequency. As demonstrated before, when HRDR dampers are designed, A_v and h_v are determined and the main further step is determining the storage modulus G_1 and the loss factor η using damper analysis/testing results. These two parameters are affected by environmental temperature and excitation frequency. In order to depict these effects, some mathematical models are proposed. The main models are considered as Kelvin model (Gluck et al., 1996), Maxwell model (Zhang and Soong, 1992), the standard linear solid model (Inaudi,1996), complex stiffness model (Markis, 1994), four parameters model (Kasia et al., 1993), and the finite element model (Tsai, 1994). Among these mathematical models, only the finite element model can simulate temperature and frequency effects simultaneously, and this model is very complex. Herein, a new mathematical model as the equivalent standard solid model is proposed, which is based on the standard linear solid model and

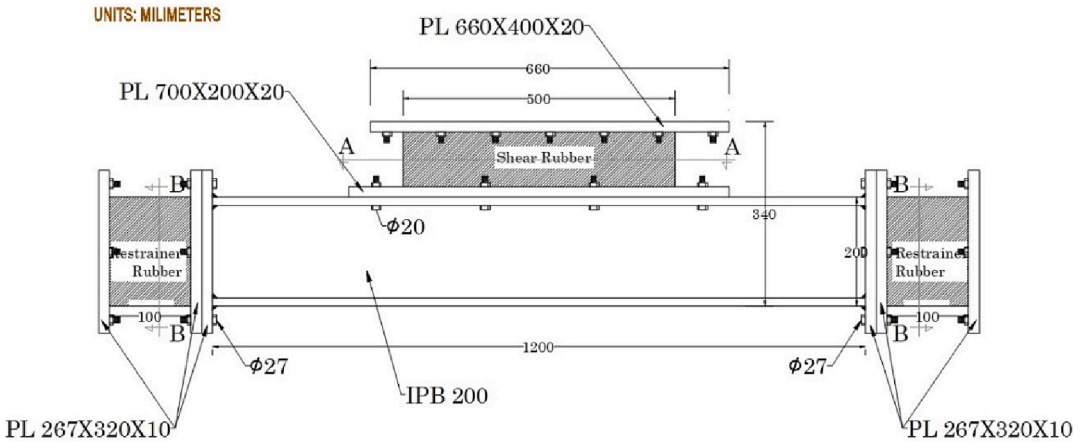

Fig. 8. Dimension specimen of simulating the proposed HRDR system.

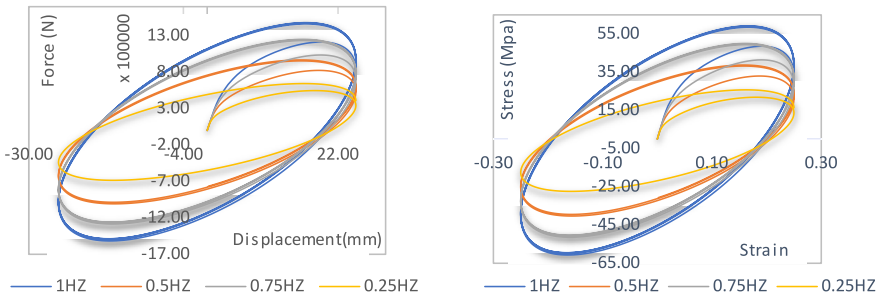

(a) Hysteresis Plot (force displacement response) (b) Stress – Strain Response

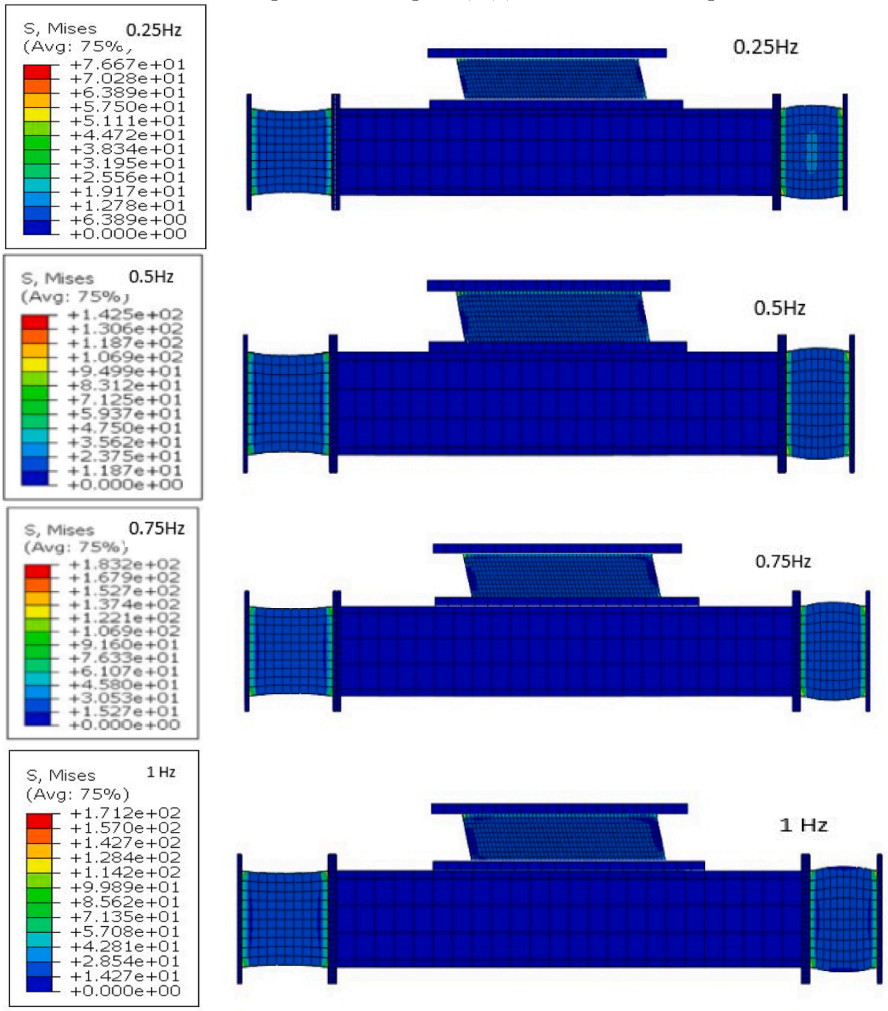

(c) Principal stress counter in various frequencies (0.25,0.5,0.75 and 1 Hz)

Fig. 9. Response of HRDR device under applied cyclic load with 25% rubber thickness strain amplitude.

temperature-frequency equivalent theory.

In order to evaluate performance of HRDR dampers, the energy dissipation capacity of the damper is need to calculate. For this purpose, the characteristic parameters of HRDR damper device include of the storage modulus G_1, the loss modulus G_2 and the loss factor η are required to be determined from the hysteresis response of damper device under applied cyclic loads, as shown in Fig. 8. The ellipse hysteresis loop of HRDR dampers can be expressed as following force–displacement relationship:

$$\left(\frac{F_d - K_{d1}u_d}{\eta K_{d1}u_0}\right)^2 + \left(\frac{u_d}{u_0}\right)^2 = 1 \tag{13}$$

where F_d and u_d are force and displacement of the device, K_{d1} is the storage stiffness, ($K_{d1} = \frac{F_1}{u_0}$), F_1 is the damping force at the maximum displacement, as shown in Fig. 7.

In accordance with the excitation mitigation theory of VE dampers [30], the storage modulus G_1, the loss modulus G_2, the loss factor η and energy dissipation E_d can be obtained by the following equations:

$$G_1 = \frac{F_1 h_v}{A_v u_0} \tag{14}$$

$$\eta = \frac{F_2}{F_1} \tag{15}$$

$$G_2 = \eta G_1 \tag{16}$$

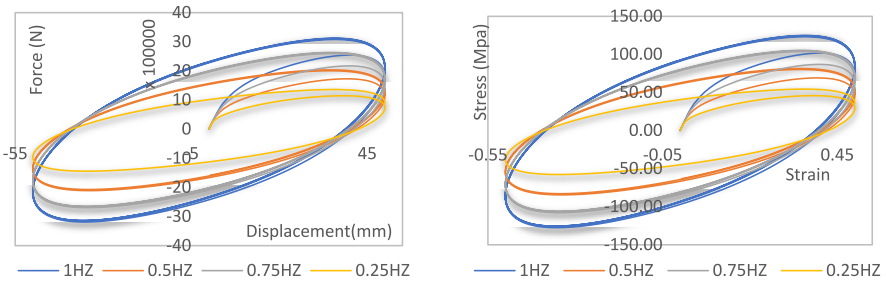

(a) Hysteresis Plot (force displacement response) (b) Stress – Strain Response

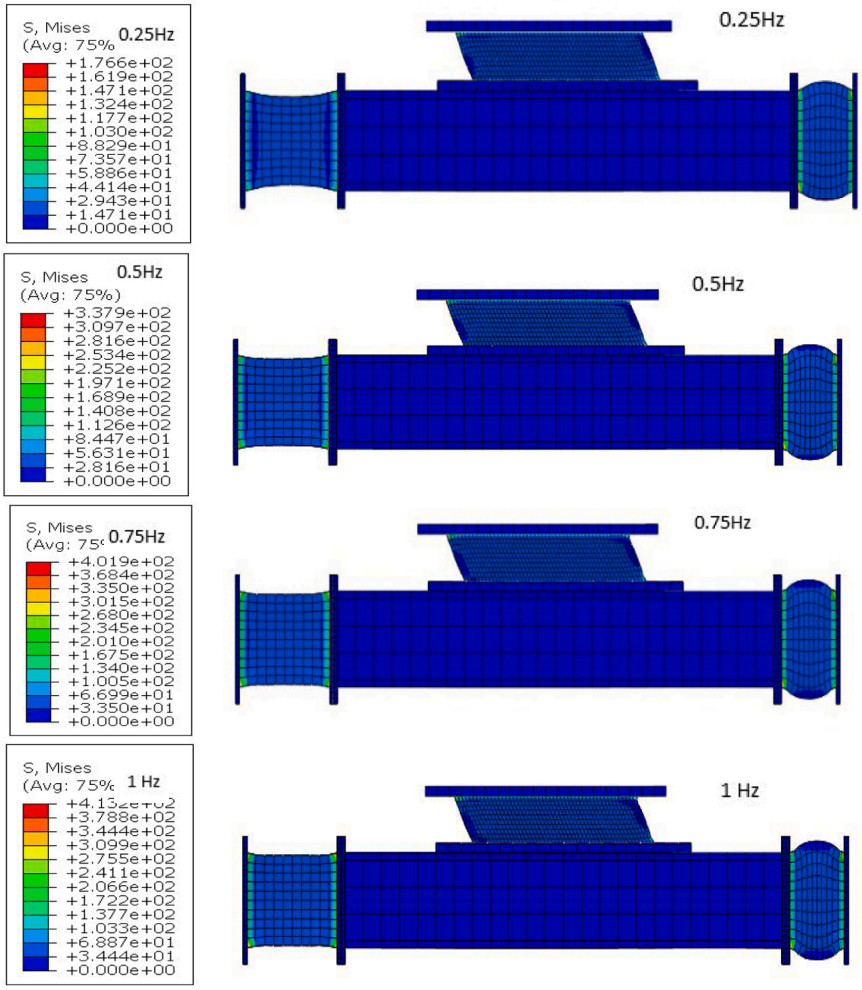

(c) Principal stress counter in various frequencies (0.25,0.5,0.75 and 1 Hz)

Fig. 10. Response of HRDR device under applied cyclic load with 50% rubber thickness strain amplitude.

$$E_d = \frac{\pi G_2 A_v u_0^2}{h_v} \tag{17}$$

where F_2 is the damping force at the zero displacement and calculate using following equation:

$$F_2 = \eta K_{d1} u_0 \tag{18}$$

The dimensional parameters of the HRDR damper is already known (as designed) and F_1, F_2 can be determined from the hysteresis curves, then the storage modulus G_1, the loss modulus G_2, the loss factor η and energy dissipation E_d of the device can be obtained. Furthermore, the equivalent stiffness (K_d) and the equivalent damping (C_d) of the HRDR device can be calculated using Equations (10) and (11).

In order to evaluate performance of the proposed HRDR system at different frequencies, the finite element model of HRDR device has been developed and subjected to cyclic loads with amplitude of 25%, 50%, 100% and 150% rubber thickness strain in various frequencies. For this purpose, the initial design of HRDR is considered as shown in the Fig. 8 and finite element model is developing accordingly. In order to simplify numerical modeling process, the bolts connections are defined as tie constraint during finite element modeling to connect various components.

The force–displacement results as hysteresis curves for the HRDR damper and stress state (stress contour) in various components of the HRDR device during its functioning under different excitation frequencies and amplitudes at environment temperature, are presented in

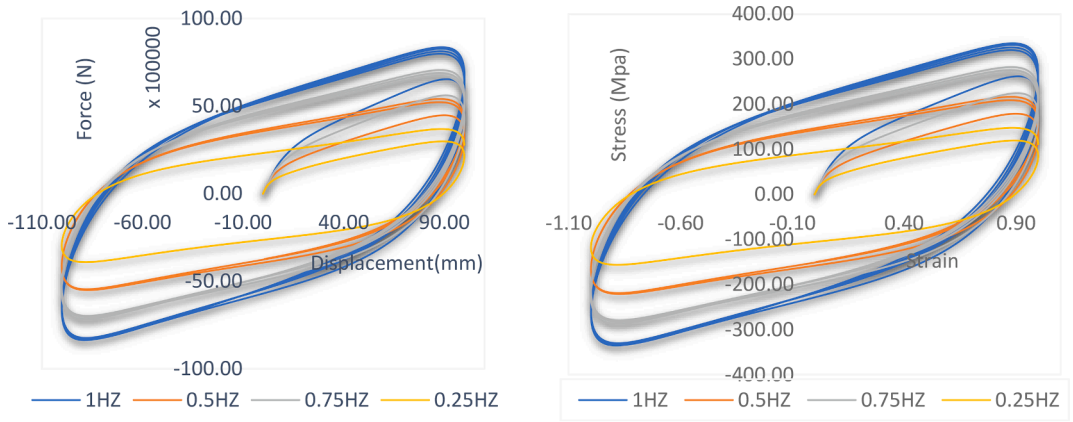

(a) Hysteresis Plot (force displacement response) (b) Stress – Strain Response

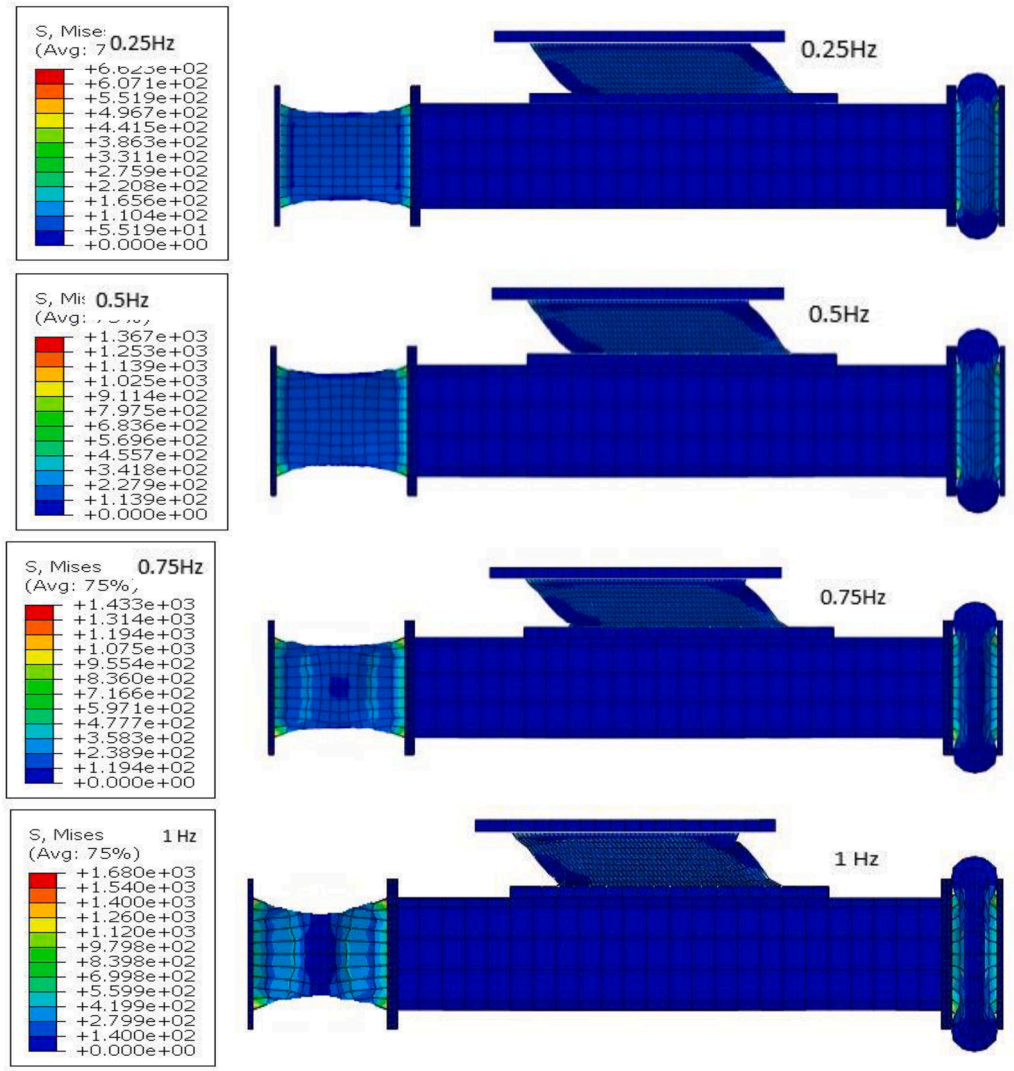

(c) Principal stress counter in various frequencies (0.25,0.5,0.75 and 1 Hz)

Fig. 11. Response of HRDR device under applied cyclic load with 100% rubber thickness strain amplitude.

Figs. 9–12. The results indicate that the slope and plump degree of these hysteresis curves are obviously different in various excitation frequencies and amplitudes. The slope and plump degree of force–displacement hysteresis curves are correlative with the stiffness and energy dissipation of the damper, respectively.

According to these figures, for all excitation frequencies, the maximum recorded force is related to the frequency of 1 Hz. According to Fig. 9, for a strain of 25% and a frequency of 0.25 Hz, the maximum force is 643 kN and for load frequencies of 0.5, 0.75 and 1 Hz, the peak damping force is obtained as 968, 1250 and 1480 kN, respectively. These results indicate that as expected, the generated damping force by the HRDR device improves by 50%, 94% and 130% when the frequency

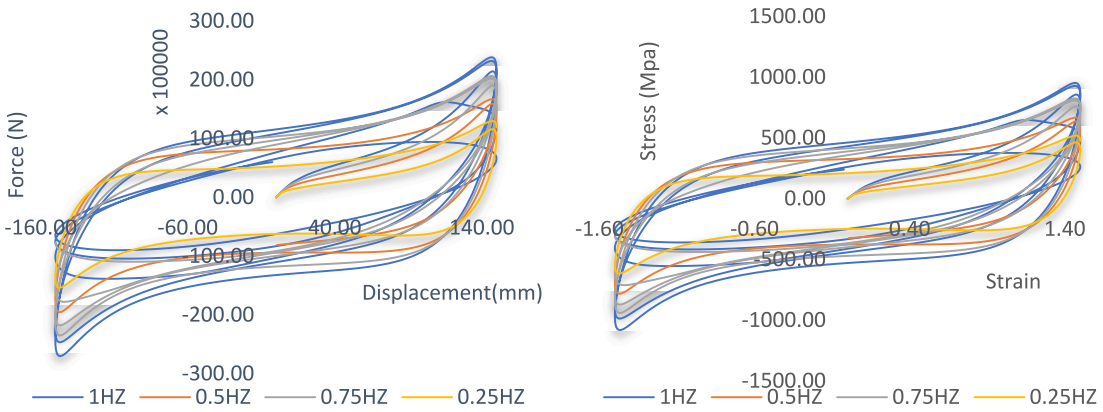

(a) Hysteresis Plot (force displacement response) (b) Stress – Strain Response

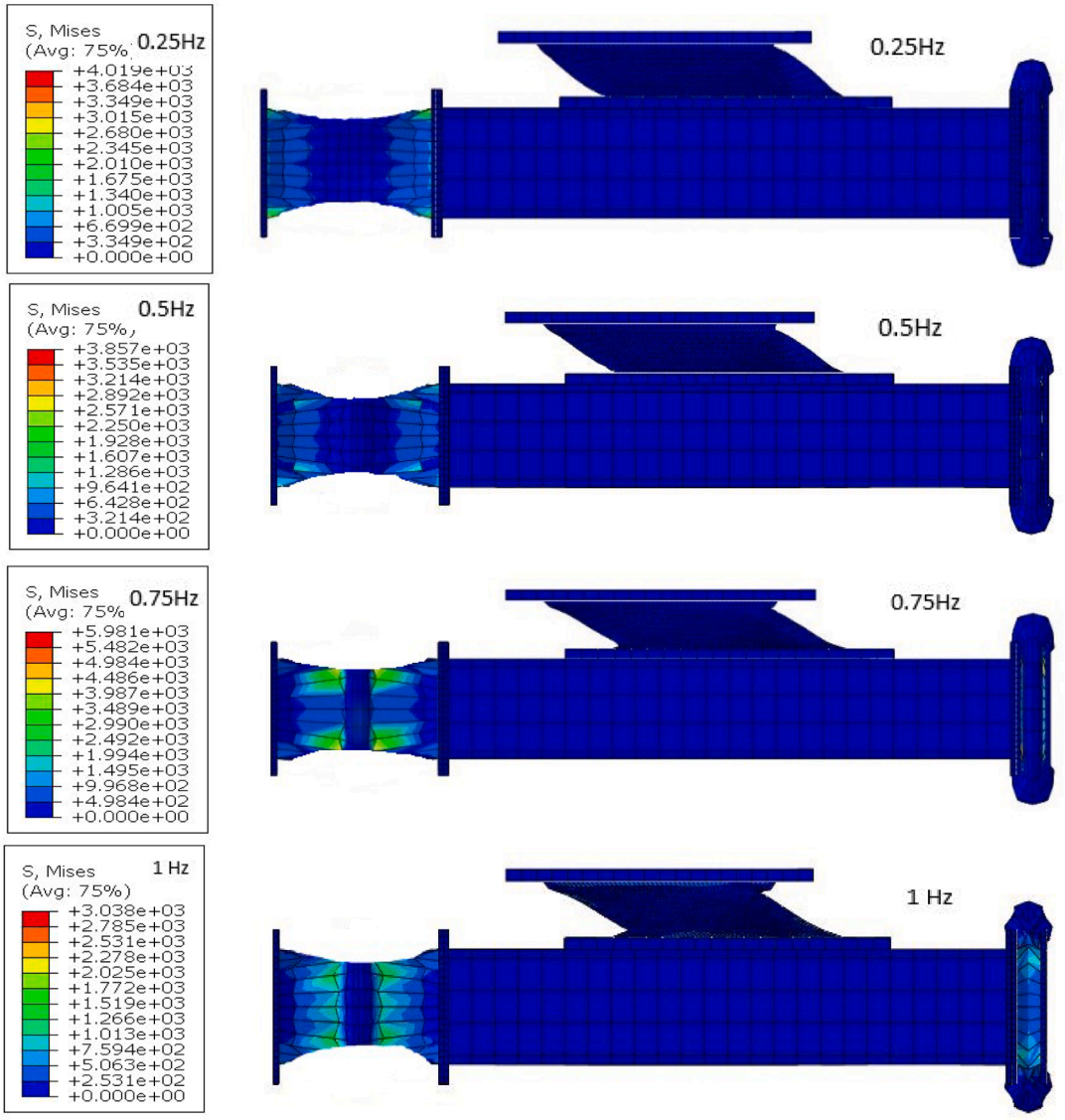

(c) Principal stress counter in various frequencies (0.25,0.5,0.75 and 1 Hz)

Fig. 12. Response of HRDR device under applied cyclic load with 150% rubber thickness strain amplitude.

Table 10
Parameters related to performance of the device under different conditions.

f_{hz} Frequency	A_m Disp. Amplitude	F1 damping force at the maximum displacement	F2 damping force at the zero displacement	G1 Storage modulus	η Loss factor	G2 Loss modulus	Ed Energy dissipation
(Hz)	(mm)	(KN)	(KN)	(MPa)		(MPa)	(KN.m)
0.25	25	544	643	44	1.182	51	50
0.50		804	968	64	1.204	77	76
0.75		985	1250	79	1.269	100	98
1		1117	1480	89	1.325	118	116
0.25	50	1124	1360	90	1.210	109	107
0.50		1663	2035	133	1.224	163	160
0.75		2043	2632	163	1.288	211	207
1		2423	3122	194	1.288	250	245
0.25	100	2636	3697	211	1.403	296	290
0.50		3748	5411	300	1.444	433	425
0.75		4872	7059	390	1.449	565	554
1		5704	8369	456	1.467	670	657
0.25	150	6213	12,992	497	2.091	1039	1020
0.50		6409	16,703	513	2.606	1336	1311
0.75		6897	20,638	552	2.992	1651	1620
1		7895	23,821	632	3.017	1906	1870
0.25	SHEAR LAYER ONLY	573	959	46	1.674	77	75
0.50	100 mm	886	1430	71	1.614	114	112
0.75		1091	1784	87	1.635	143	140
1		1368	2127	109	1.555	170	167

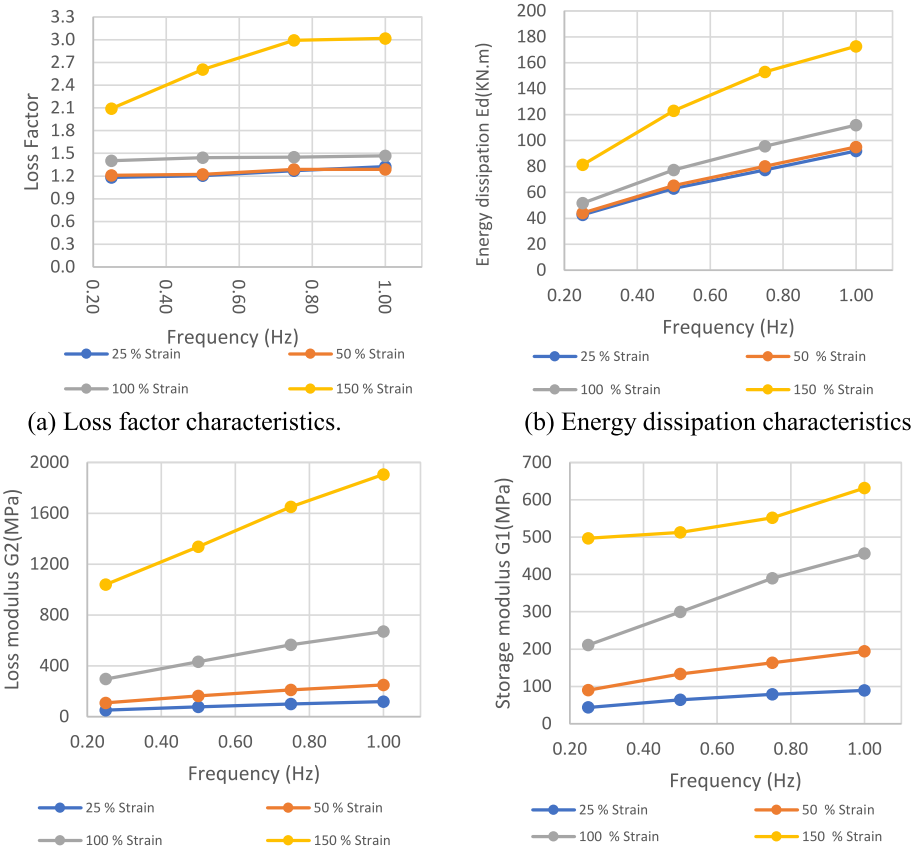

(a) Loss factor characteristics.

(b) Energy dissipation characteristics

(c) Loss modulus characteristics.

(d) Storage modulus characteristics

Fig. 13. Numerical results comparison under different frequencies (0.2 Hz to 1 Hz) for various deformations (25% to 150% rubber thickness strain).

of applied load increases from 0.25 Hz to 0.5 Hz, 0.75 Hz and 1 Hz, respectively, which is due to better performance of the high damping rubber material when subjected to the higher load frequencies.

Accordingly, due to the increase in the area under the hysteresis curve, the amount of energy absorbed by the damping system for the frequency of 1 Hz, has the highest value compared to other loading frequencies. Similar results have been obtained when cyclic displacement with amplitude equivalent of 50%, 100% and 150% rubber strain have been applied to the HRDR device as shown in Figs. 9 to 12. In parts c and d of Figs. 9 to 12, deformation of various components of HRDR device and Von Mises stress contours for various components of HRDR device are presented during applied loads for various load frequencies of

Table 11
Damping and stiffness of the device under different conditions.

f_{hz} Frequency	A_m Disp. Amplitude	F1 damping force at the maximum displacement	F2 damping force at the zero displacement	G1 Storage modulus	H Loss factor	C_d Equivalent damping	Kd Equivalent stiffness
(Hz)	(mm)	(KN)	(KN)	(MPa)	–	(KN.sec/mm)	(KN/mm)
0.25	25	544	643	44	1.182	103	22
0.50		804	968	64	1.204	155	32
0.75		985	1250	79	1.269	200	39
1		1117	1480	89	1.325	237	45
0.25	50	1124	1360	59	1.210	143	29
0.50		1663	2035	92	1.224	225	46
0.75		2043	2632	122	1.288	314	61
1		2423	3122	142	1.288	367	71
0.25	100	2636	3697	171	1.403	478	85
0.50		3748	5411	265	1.444	765	132
0.75		4872	7059	349	1.449	1012	175
1		5704	8369	405	1.467	1189	203
0.25	150	6213	12,992	802	2.091	3353	401
0.50		6409	16,703	1278	2.606	6661	639
0.75		6897	20,638	1617	2.992	9677	809
1		7895	23,821	1773	3.017	10,699	887
0.25	SHEAR LAYER ONLY	573	959	46	1.674	153	23
0.50	100 mm	886	1430	71	1.614	229	35
0.75		1091	1784	87	1.635	285	55
1		1368	2127	109	1.555	340	47

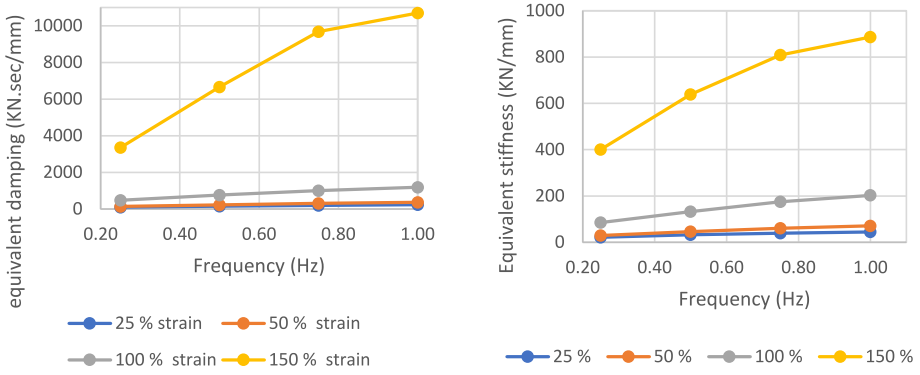

(a) Equivalent damping characteristics. (b) Equivalent stiffness characteristics

Fig. 14. Equivalent damping and stiffness results comparison under different frequencies (0.2 Hz to 1 Hz) and deformations (25% to 150% rubber thickness strain).

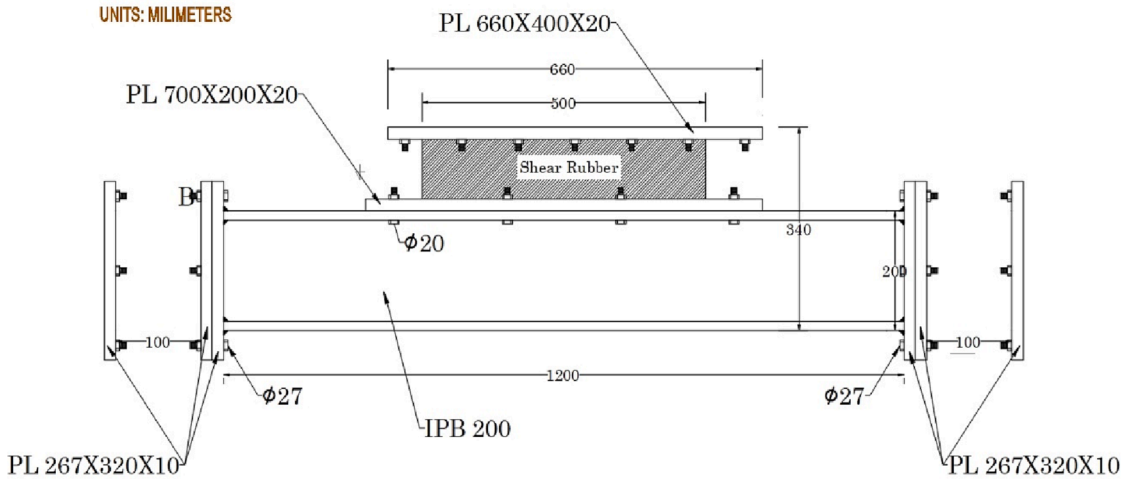

Fig. 15. Dimension specimen of simulating the proposed HRDR system without restrainer rubber.

Table 12
Effective stiffness of the device under different conditions in compression with shear rubber only.

Frequency (Hz)	Disp. Amplitude (mm)	F1 N	F2 N	Storage modulus G1(MPa)	loss factor	Equivalent damping (KN.sec/mm)	Equivalent stiffness (KN/mm)
0.25	100	2636	3697	171	1.403	478	85
0.50		3748	5411	265	1.444	765	132
0.75		4872	7059	349	1.449	1012	175
1		5704	8369	405	1.467	1189	203
0.25	SHEAR LAYER ONLY 100 mm	573	959	46	1.674	153	23
0.50		886	1430	71	1.614	229	35
0.75		1091	1784	87	1.635	285	55
1		1368	2127	109	1.555	340	47

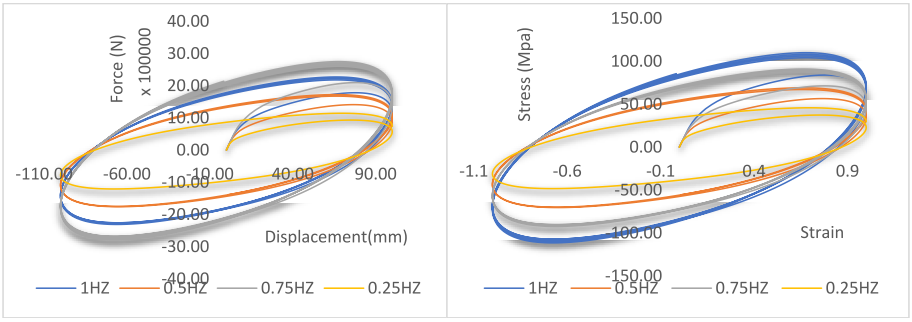

(a) Hysteresis Plot (force displacement response) (b) Stress – Strain Response

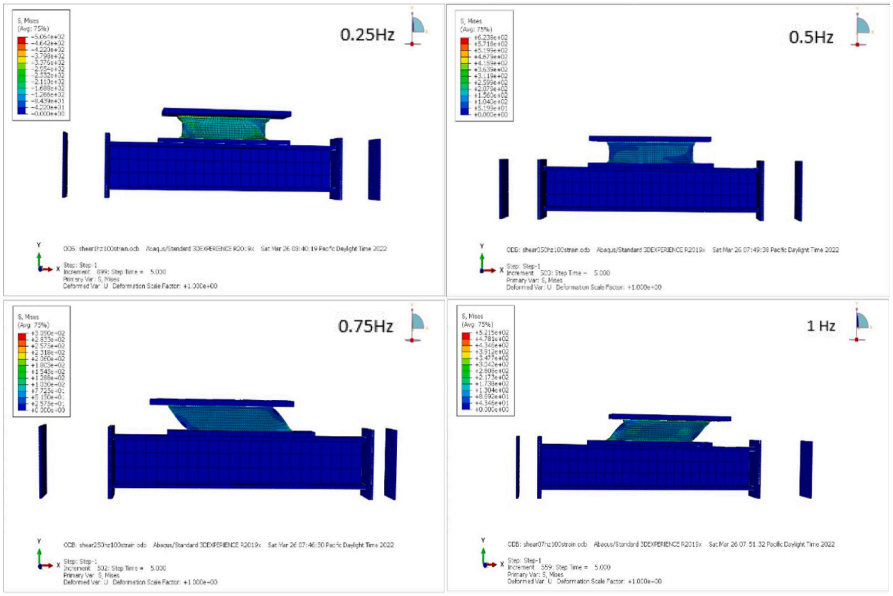

(c) Principal stress counter in various frequencies (0.25,0.5,0.75 and 1 Hz)

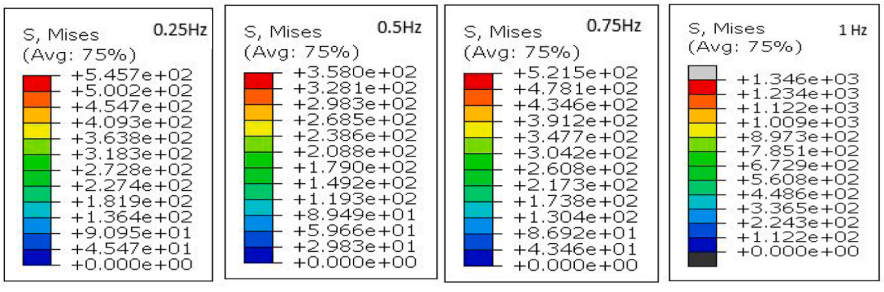

(d) numerical results of stress in various frequencies (0.25,0.5,0.75 and 1 Hz)

Fig. 16. Response of HRDR device under applied cyclic load with 100% rubber thickness strain amplitude by consider of shear layer only (high damping part without hyper-elastic rubber components in both sides).

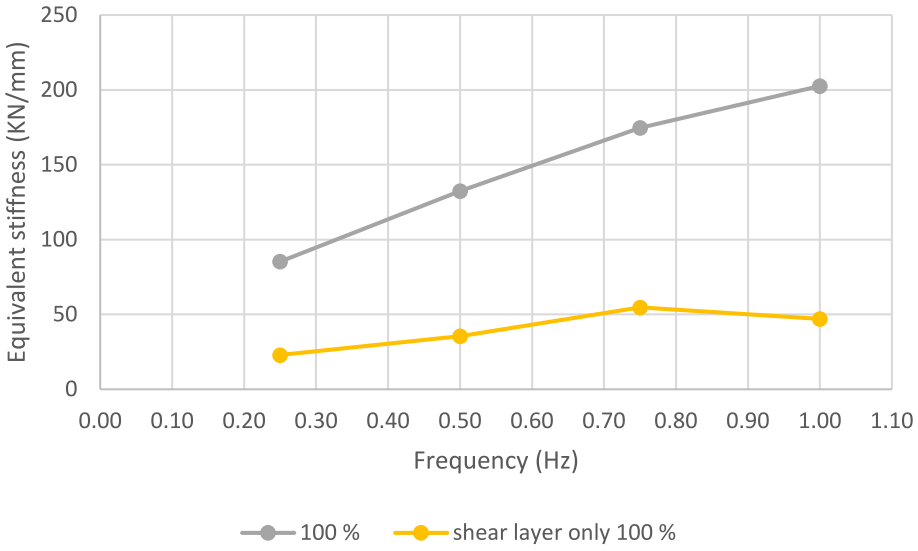

Fig. 17. Equivalent stiffness results comparison with shear layer only for various frequencies (0.25 Hz to 1 Hz) and deformations (100% rubber thickness strain).

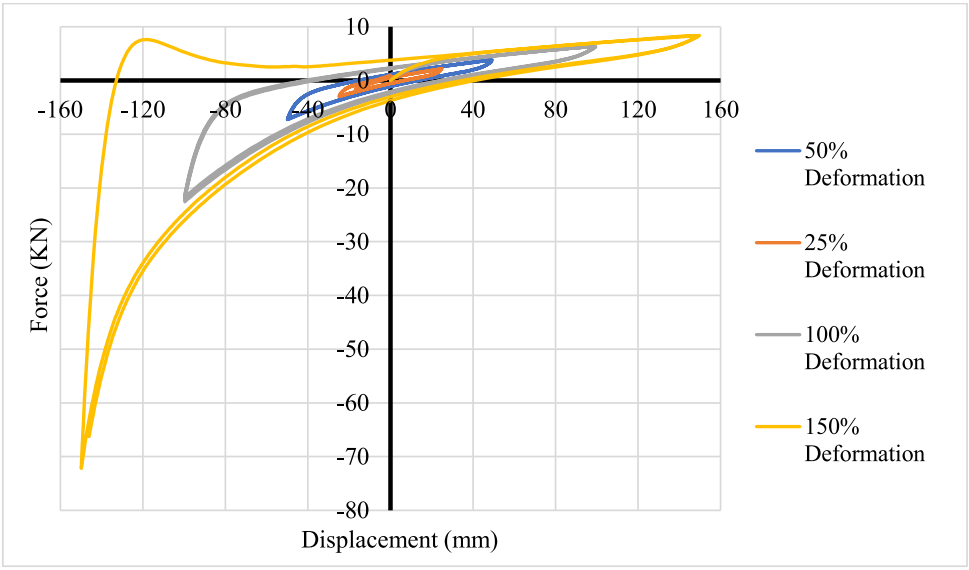

Fig. 18. Hysteresis response for restrainer in compression and tension for various deformation rates.

Table 13
Maximum compression and tension forces for restrainer rubber under cyclic loads.

	25% rubber thickness strain	50% rubber thickness strain	100% rubber thickness strain	150% rubber thickness strain
T (Max)	2.17	3.83	6.39	8.38
P (Max)	−2.96	−7.26	−22.56	−72.18

0.25 Hz to 1 Hz. As it was expected, when the rigid beam moved to the right side due to applied loads, the high damping rubber (viscoelastic) component experiences shear deformation and restrainer rubber (hyper elastic) component at the right side is compressed.

Accordingly, the damping force is generated by the high damping rubber component to dissipate vibration energy and the restraining force is produced by the restrainer rubber component to restrain movement. Hence, the restrainer rubber (hyper elastic) component at the left side is expanded due to pulling force and catered small amount of restraining force. By changing direction of the movement (moving to left), the high damping rubber is shifted to the left side and the restrainer rubbers at left and right sides are compressed and expanded respectively.

As can be seen in these Figures, with increase in the load frequency for deformation corresponding to 25%, 50% and 100% strains, the Von Mises stress value increases. Thus, as a consequent for deformation of 25% strain, the stress value increases from 76.67 MPa at a frequency of 0.25 Hz to 171.2 MPa at the frequency of 1 Hz. This increment was about 140% for 50% and 100% strains. Therefore, these results indicated that when performance of HRDR increases in higher frequencies to generate more damping force, the greater stress is developed in the rubber components. However, for deformation of 150% strain, this issue is slightly different, so that the lowest value of stress has been recorded for the frequency of 1 Hz as 3038 MPa and the highest stress has been

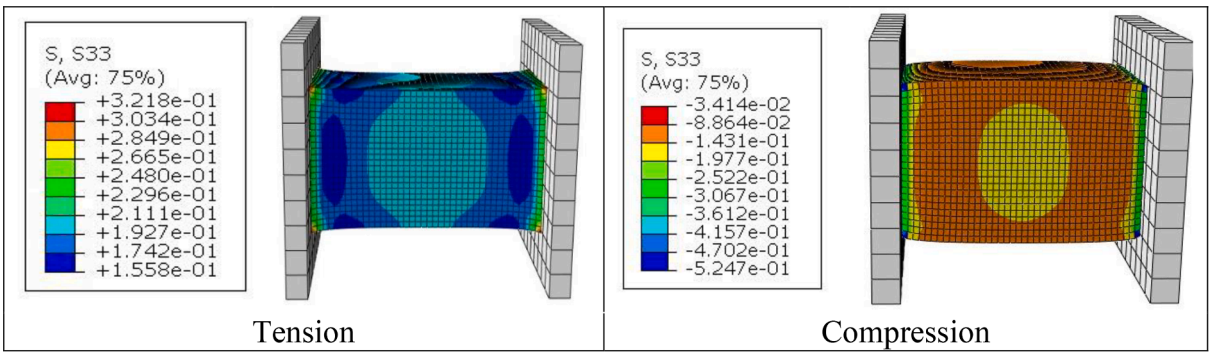

(a): 25% Strain

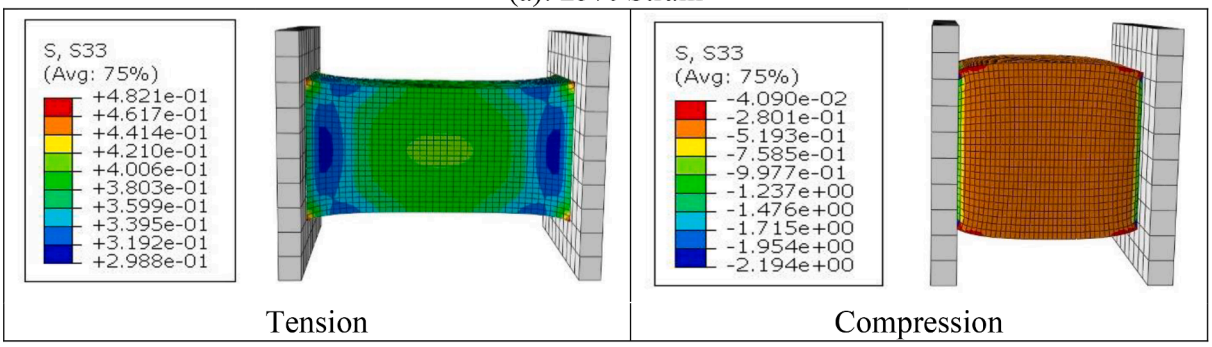

(b): 50% Strain

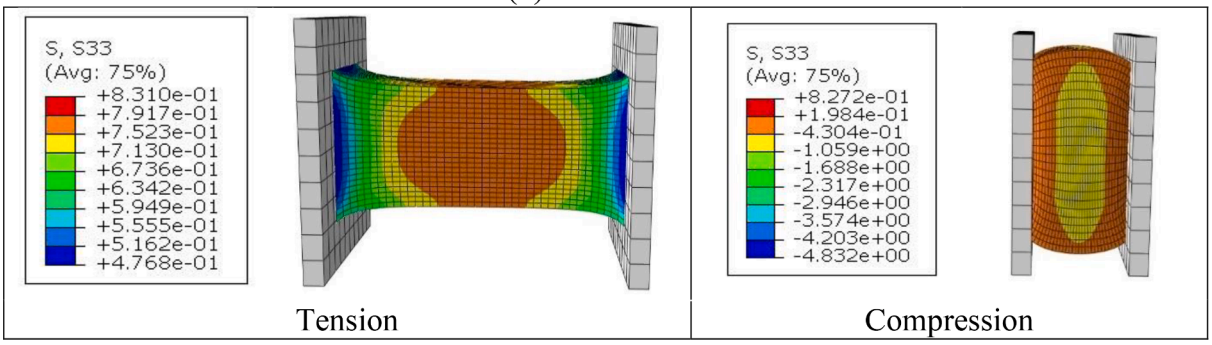

(c): 100% Strain

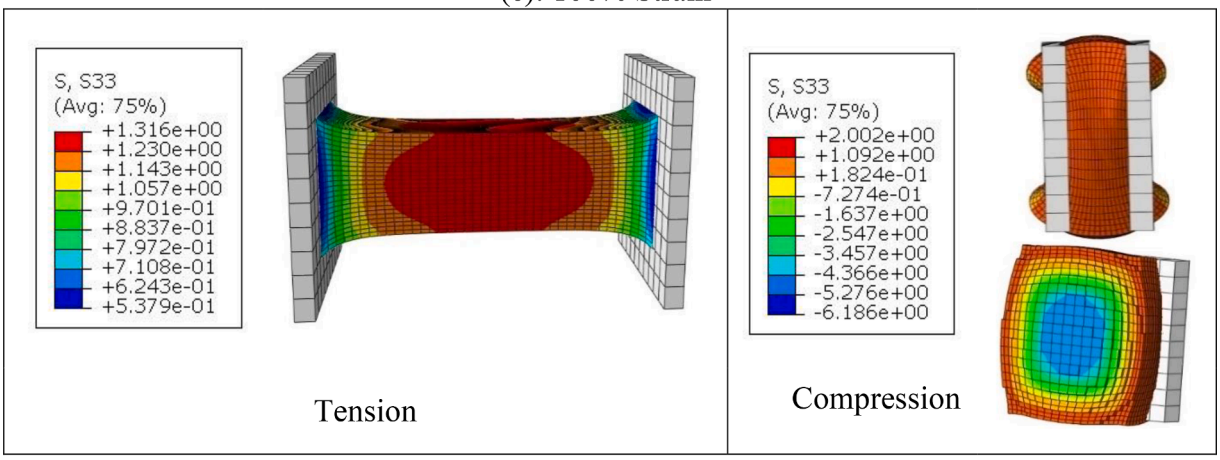

(d): 150% Strain

Fig. 19. Stress of restrainer rubber under compression and tension load at various strain.

observed for load frequency corresponds to the 0.75 Hz as 5981 MPa. Also, for the load frequencies of 0.25 and 0.5 Hz, the stress at 150% strain was 4019 and 3857 MPa, respectively. According to the stress contours presented in Figs. 9 to 12, most of high stresses occurred in the high damping component for high excitation frequencies (0.75 and 1 Hz).

It is worthy to highlight that for small strain ranges (25 % and 50 %), both rubber components (viscoelastic and hyper elastic rubbers) remain in the elastic state and act linearly, while according to Figs. 11 and 12, for the strain of 100% and 150%, the function of high damping rubber

Table 14
Modification factor for aging by EN1998-PART 2.

Component	Equivalent damping coefficient ξ	Equivalent shear modulus at 100% of strain G	$\lambda_{max,\,f1}$	
			K_P	F_0
HDRB	$\xi \leq 0.15$	G > 0.5 MPa	1.2	1.2
	$\xi > 0.15$	G > 0.5 MPa	1.3	1.3

and restrainer rubber entered the non-linear region and show the inelastic and plastic behavior. This issue can be seen from the shape of the hysteresis curves in parts a and b, as well as the shape of the restraining rubbers and shear rubber shown in parts c and d of Figs. 9 to 12.

Parameters related to the performance of the HRDR dampers under different load frequencies in the range of 0.25 Hz to 1 Hz and displacement amplitudes of 25%, 50%, 100% and 150% rubber thickness strain are calculated and listed in Table 10 and plotted in Fig. 13. As expected, the results corresponding to the storage module, loss module and energy dissipation module for deformation of 150% strain are considerably higher than the other applied lower deformations (20%, 50% and 100% thickness) in all studied load frequency ranges. This is indicating the superior performance of the HRDR device to dissipate vibration effect when it is subjected to the higher deformations due to rubber damping action.

Moreover, based on the results, the storage modulus (G_1), the loss modulus (G_2) and accordingly, the energy dissipation (E_d) of the device augment with increasing the frequency of the applied load. Further, the results revealed that energy dissipation capacity of the HRDR device is higher when the applied load frequency is increased. This is more obvious when device is subjected to deformation of 150% strain with 0.25 Hz frequency in comparison to 1 Hz frequency with increment of 127% for storage module, 184% for loss modules and 184% for energy dissipation module. However, the loss factor η increases with increase of load frequency about 12% from 0.25hz to 1 Hz in 25% strain, and about 7% from 0.25hz to 1 Hz in 50% strain, and about 5% from 0.25hz to 1 Hz in 100% strain, and about 44% from 0.25hz to 1 Hz in 150% strain. In total, the results prove that the proposed HRDR system has a considerable energy dissipation capacity and as it is presented in Table 10, the highest energy absorption is related to the displacement equivalent to 150% strain with loading frequency of 1 Hz.

The equivalent damping and stiffness values of the HRDR device are also calculated for various applied deformations and load frequencies based on Equations 10 and 11as presented in Table 11 and results

Table 16
Rubber properties (BS 5400 Part9.1&2).

Property	Requirement according to B.S. 5400 Part 9.1 & 2
Hardness	56–65 IRHD
Tensile strength (min)	15.5 MPa
Elongation at break (min)	400 %
Compression set, Max (24 h / 100 °C)	30 %
UV Stabilised	No Crack
Ozone resistance	No

Table 15
Modification factor for temperature by EN1998-PART 2.

Component	Equivalent damping coefficient ξ	Equivalent shear modulus at 100% of strain G	$\lambda_{max,\,f2}$							
			K_P Design temperature				F_0 Design temperature			
			−20	−10	0	20	−20	−10	0	20
HDRB	$\xi \leq 0.15$	G > 0.5 MPa								
	$\xi > 0.15$	G > 0.5 MPa								

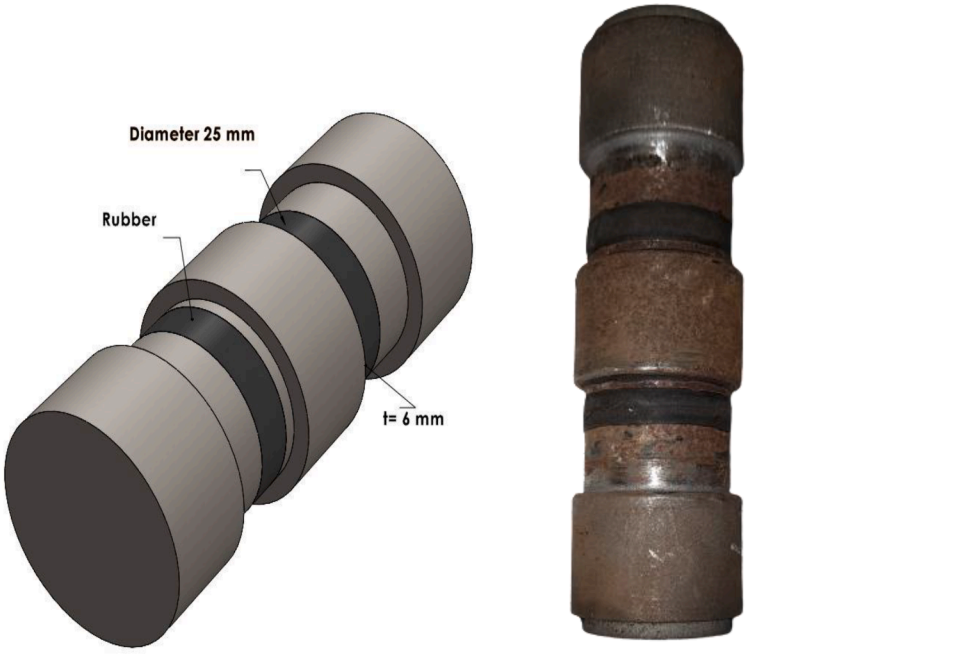

(a) thickness and diameter of rubber (b) Real manufactured specimen for experimental test

Fig. 20. A double shear rubber cylindrical specimen (ASTM D429).

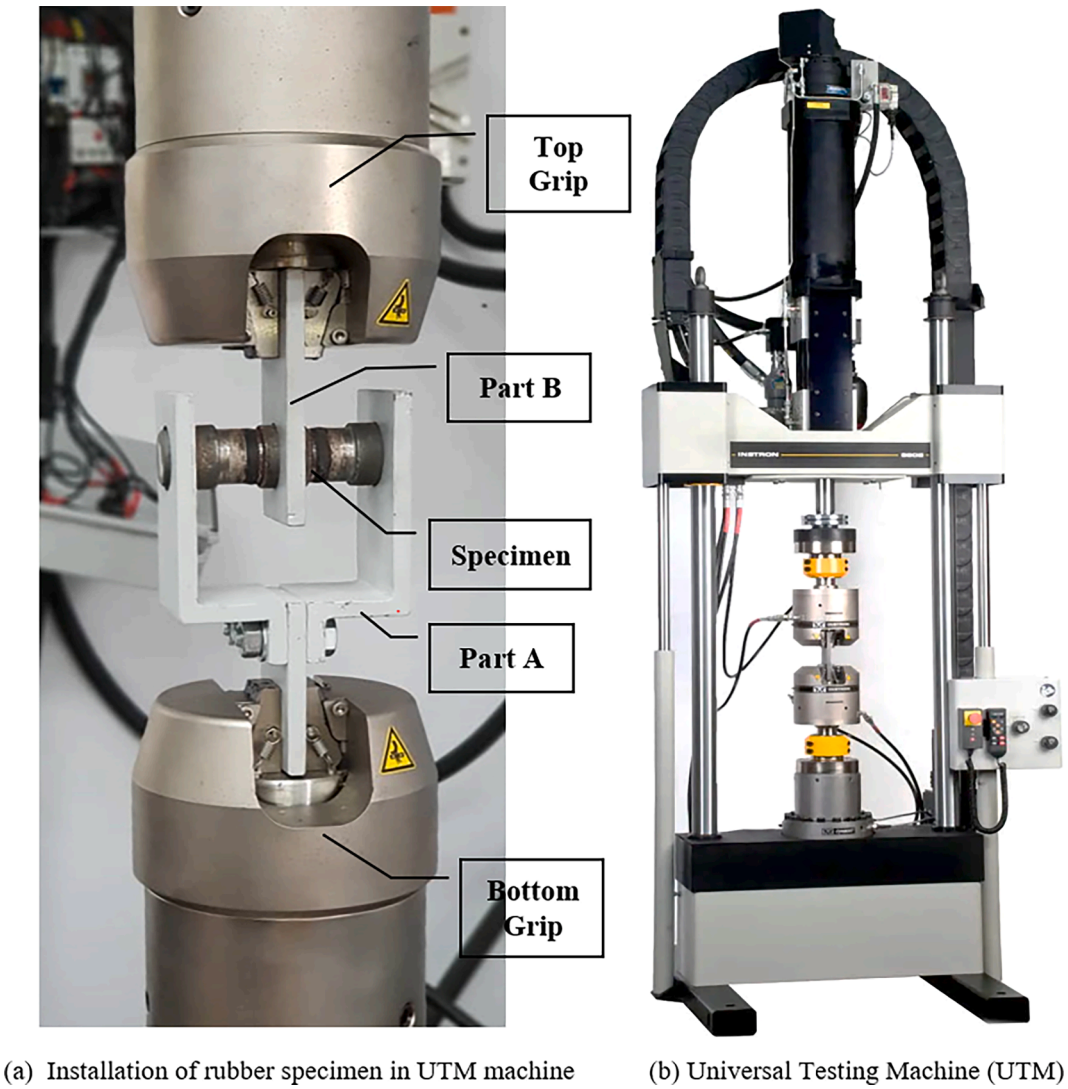

Fig. 21. Testing setup for double shear rubber cylindrical specimen (ASTM D429).

depicted in Fig. 14.

According to these results, the equivalent damping corresponding to all 25%, 50%, 75%, 100% and 150% strains, increases by increase of loading frequency. However, the increment is about 130% at low frequencies (0.25 and 0.5 Hz and 0.75 Hz) and about 220% at high frequencies (1 Hz). Accordingly, the equivalent stiffness increases in all cases when the loading frequency increases. It can be understood from Table 11 that the equivalent stiffness increases with increase of load frequency about 105% from 0.25hz to 1 Hz in 25% strain, and about 140% from 0.25hz to 1 Hz in 50% strain, and about 130% from 0.25 Hz to 1 Hz in 100% strain, and about 120% from 0.25hz to 1 Hz in 150% strain.

In order to investigate the effect of restrainer components, the device without the presence of restrainer rubber parts have been modeled (Fig. 15) and analysis has been conducted by applying displacements equivalent to 100% strain. Accordingly, the results are listed in Table 12 and presented in Figs. 16 and 17. It can be seen from Table 12 that the energy dissipation and equivalent stiffness decreased in all frequencies for model without restrainer rubber about 75% and 95%, respectively. Therefore, these results proved the effect of restrainer rubber components in increasing the energy dissipation and the equivalent stiffness of the proposed HRDR system besides its own function as restrainer system to limit and prevent the large deformations. Accordingly, the stress distribution in the HRDR device during movement of the rigid beam under applied load has been shown in the same Figure. Based on the results, the maximum stresses occurred in the high damping rubber (visco-elastic) component which is indicating substantial action of HDR to dissipate the vibrations.

4.1. *The compression and tensile deformation of restrainer rubber*

The restrainer has been subjected to the cyclic loads with deformations corresponding to 25%, 50%, 100% and 150% strain of rubber thickness of the restrainer and the hysteresis responses in compression and tension have been plotted in Fig. 18 and results are tabulated in Table 13.

As it was expected, the rubber generated more resistant force in compression in comparison to the tension state. This difference is more obvious when rubber has been subjected to higher strains such as 100% and 150% of rubber thickness due to its inelastic behaviour.

Based on the results presented in Table 13, this difference was only 36% higher force in compression when rubber has been deformed about 25% strain of rubber thickness, but by increasing of deformation of rubber to 100% and 150% of its strain, the difference between compression force of rubber and tension force is almost 7.6 times. Also, the results proved that by increase of rubber deformation, its resistant force is increasing in both compression and tension situation. Although, as described in above, this increment is highly noticeable when rubber in

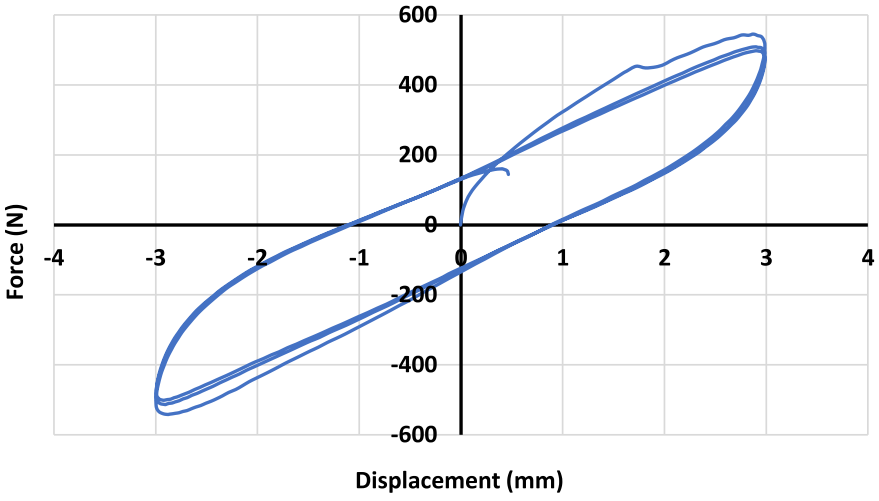

(a) Testing results for 6mm displacement amplitude (50% strain)

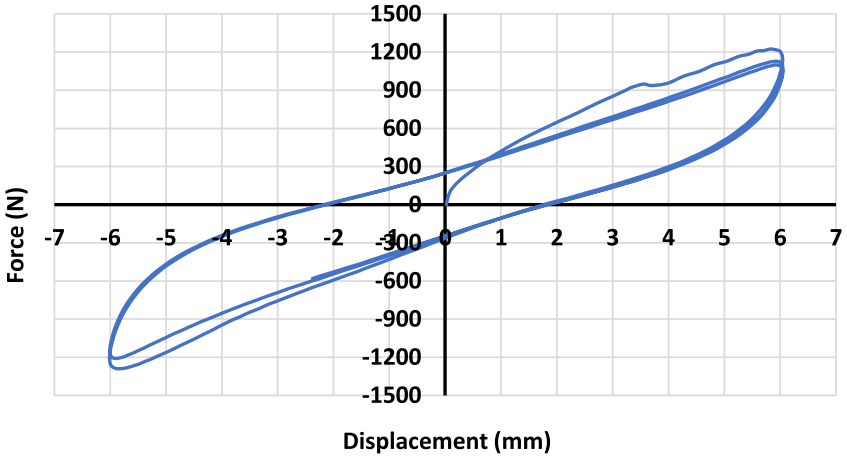

(b) Testing results for 9mm displacement amplitude (100% Strain)

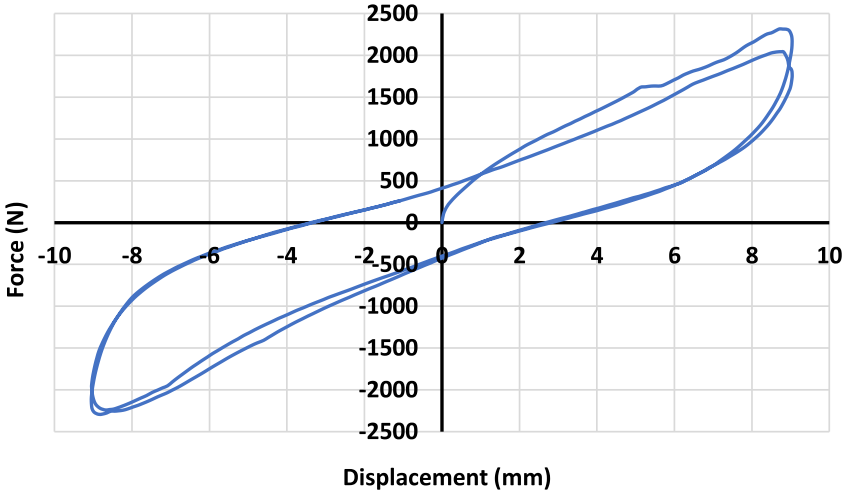

(c) Testing results for 12mm displacement amplitude (150% Strain)

Fig. 22. Results of testing double shear rubber cylindrical specimen.

compression has been applied to higher strain such as 150% strain. For the considered restrainer model, the resistant force corresponding to deformation of 150% rubber strain is 72 kN which is 2.2 times higher than generated force in 100% deformation which is 22kN only and also 23 times more in comparison of 25% deformation. Therefore, it can be concluded that rubber exhibiting its high resistant force capacity in compression condition through experiencing of deformation higher than 100% strain of rubber thickness. Thus, it is more economy to design restrainer device to function in higher deformation to use full capacity of rubber to generate restrainer force.

The stress distribution in the rubber of restrainer in compression and tension for deformation corresponding to 25%, 50%, 100% and 150%

Table 17
Results of experimental test on double shear rubber cylindrical specimen.

Disp. Amplitude (mm)	Elongation (%)	F1 Damping force at the maximum displacement (N)	F2 Damping force at the zero displacement (N)	G1 Storage modulus (MPa)	η Loss factor	Equivalent Damping (N.Sec/mm)	Equivalent stiffness (N/mm)	Shear stress MPa
3	50	497	122	2.03	0.25	40.67	165.67	1.01
6	100	1019	255	2.08	0.25	42.50	169.83	2.08
9	150	1764	410	2.40	0.23	45.56	196.00	3.60

Table 18
Researches about testing rubber under high deformations.

No	Author	Year	Elongation (%)	Maximum Measured Stress at failure stage
1	MIKI PULLEY [31] (PAGE 626)	2022	100% ~ 1000%	3 ~ 29 MPa
2	Janusz Datta, Paulina Kosiorek [32]	2016	984%	18.3 MPa
3	Bentang Arief Budiman, Poetro Lebdo Sambegoro [33]	2020	430%	20.2 MPa
4	Yun Zhou, Dingbin Li, Fei Shi, Weili Luo, Xuesong Deng [34]	2021	400%	No debonding
5	Li Han, Tian Shengze, Dang Xinzhi, Yuan Wancheng [35]	2020	300%	No debonding
6	V. S. Pawar, R. S. Pant & P. J. Guruprasad [36]	2019	225%	18 MPa
7	BSc. Sudhir Kumar [37]	2014	120%	No debonding
8	Xuan Dai Nguyen, Lotfi Guizan [38]	2021	150%	3.65 MPa
9	Takafumi Fujita [39]	1991	300%	No debonding
10	Majid Shahzad, Ali Kamran, Muhammad Zeeshan Siddiqui [8]	2015	200%	No debonding

are showed in Fig. 19. As it can be seen in these results, both tensional and compressional stresses in the rubber material are increased in higher deformations. However, compression stresses in deformation corresponding to 100% and 150% rubber strain are much more than tensile stress in the same deformations. This is more highlighted in 150% deformation; compressional stresses are about 6.18 MPa which is almost 4.7 times more than tensional stress as 1.31 MPa. As it can be seen, the Fig. 19 (a), the maximum compressional stress has been occurred in the center of rubber specimen as showed in the rubber section, while the outer layer of rubber specimen experienced of tension due to applied high deformation to the rubber specimen equivalent of 1.5 times of its unreformed thickness. Therefore, these results are confirming that there is high compression and tensile deformation due to applied compression and tensile force respectively and the stress results in both compression and tensional condition are according to reasonable expectation. Specially stress results in compression in high deformation rate is confirming the capacity of rubber material to generate higher resistant force in compression in comparison to the generated force which rubber specimen is subjected to tensional load.

4.2. Proposed system property modification factors

The nominal properties of the developed Hybrid Rubber Damper-Restrainer System in this study may change due to environmental effect such as temperature or behavioral effects such as aging or repeated cycles.

For this reason, two tests for design properties of the Hybrid Rubber Damper-Restrainer System should be used in the analyses consist of Upper Bound Design Properties (UBDPs) and Lower Bound Design Properties (LBDPs) based on Annex J of EN1998-part 2. Accordingly, as listed in Table 14 and Table 15, the maximum and minimum property modification factor (λ) needs to be applied to the post elastic stiffness (K_p) and the force at zero displacement (F_0) in order to consider effect of aging and temperature respectively. Same modification factors applicable for contamination and cumulative travel. Moreover, the combination factors also may consider minimizing the probability of simultaneous occurrence of the maximum adverse effects of all factors according to EN1998-PART 2.

5. Testing the strength and bonding between vulcanized rubber and steel plates

An experimental test was conducted to assess the vulcanization strength and bonding between rubber and steel plates under large deformation, based on ASTM D429 standards. To achieve this, a double shear rubber cylindrical specimen was manufactured as shown in Fig. 20 and tested using a dynamic actuator to induce shear deformation. The dimensions of the different parts of the specimen are depicted in Fig. 20 (a).

The specimen consists of two rubber layers with a diameter of 25 mm and a thickness of 6 mm. A solid steel cylinder is positioned in the middle of the two rubber layers, with two additional steel cylinders placed on

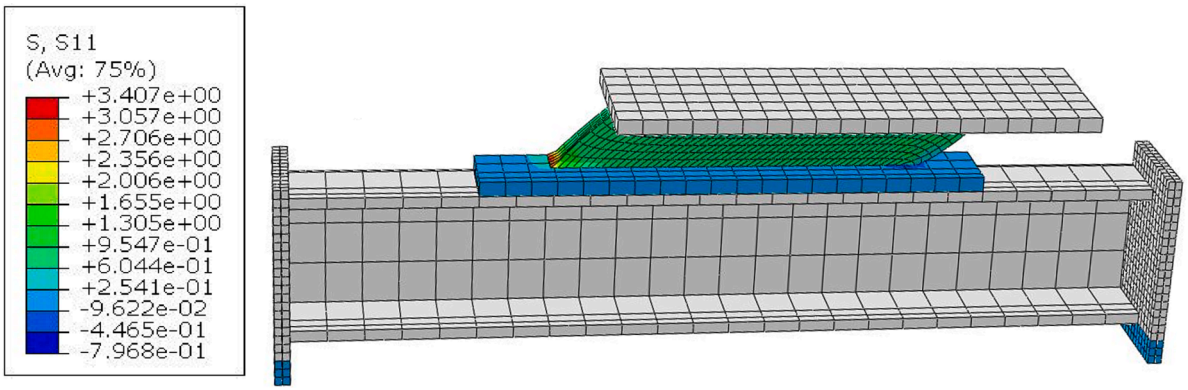

Fig. 23. Stress contour for the rubber at maximum deformation of HRDR device corresponding to 150% of rubber thickness strain.

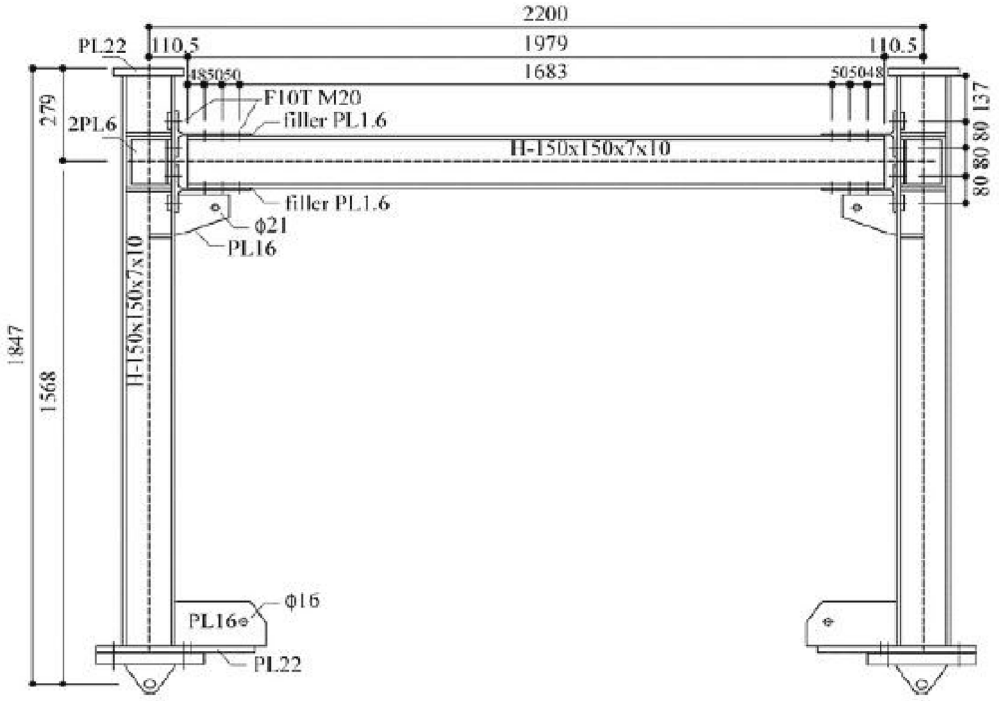

Fig. 24. Test specimens [7].

Table 19
The constitutive model for the Steel materials (elastoplastic properties).

Strain	Stress (Mpa)
0	299.0188762
0.005165	314.3193519
0.008143	330.0770358
0.013111	346.614916
0.021226	364.4544224
0.034188	384.4203484
0.054405	407.7931219
0.085137	436.5264658
0.195514	523.2171449
0.285179	591.85

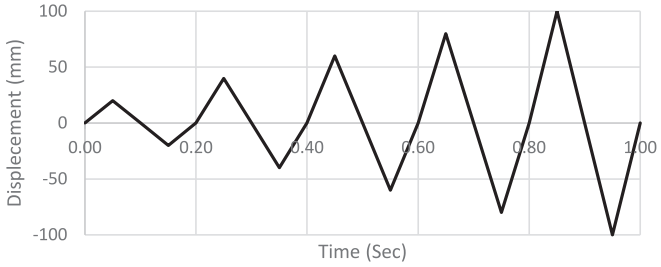

Fig. 25. Cyclic Loading Protocol.

the outer sides of the rubber layers to secure the specimen in place. The rubber material used was formulated to meet the rubber property requirements for laminated elastomeric bearings as specified in BS 5400 Part 9.1 & 2, listed in Table 16.

An apparatus has been constructed to secure the double shear cylindrical specimen in the testing machine, as shown in Fig. 21 (a). The testing apparatus consists of two parts: Part A, which is the fixed part held by the bottom grip of the testing machine and acts as a fixture for both ends of the double shear rubber cylindrical specimen, and Part B, which is the moving part held by the top grip of the testing machine. Part B facilitates the upward and downward movement of the center part of the double shear rubber cylindrical specimen. With Part A securing both sides of the specimen, the movement of the center part through Part B induces shear deformation in the rubber components on both sides.

The INSTRON Servo-hydraulic dual-axis materials testing machine (8874) with a ± 25 kN force capacity was utilized to apply dynamic movement to the specimen (Fig. 21 b) in order to examine the behavior of rubber under various deformations and assess the durability of the vulcanized bonding between the rubber and the metal.

The experimental test involved subjecting the rubber components to cyclic shear deformation with amplitudes of 3 mm, 6 mm, and 9 mm, which correspond to strain levels of 50%, 100%, and 150% of the rubber thickness, respectively. The results of testing the double shear rubber cylindrical specimen are presented in Fig. 22 for all three considered amplitudes. These graphs demonstrate that the nonlinear behavior of the rubber occurred after experiencing deformation equivalent to 100% of the rubber thickness strain.

The equivalent stiffness and damping values obtained from the hysteresis results are listed in Table 17, indicating that the shear stiffness of the rubber ranges from 165 N/mm to 196 N/mm when the specimen was tested with amplitudes of 3 mm to 9 mm. The effective damping was calculated as 40.67 N·sec/mm for an amplitude of 50% strain and increased to 45.56 N.sec/mm when a displacement with a 150% strain amplitude was applied.

Furthermore, the results revealed that the rubber experienced a shear stress of 3.6 MPa at a deformation corresponding to 150% of the rubber thickness, without any signs of debonding or delamination between the vulcanized rubber and the steel parts. The test was repeated several times under the same deformation conditions, but no cracks or indications of damage were observed. Therefore, the test demonstrated that the vulcanized rubber can function effectively even under high deformations, such as 150% strain of the thickness, without experiencing debonding.

Similar findings have been reported by numerous researchers regarding the strength of vulcanized rubber under high deformations, and some of their studies have been included in Table 18 for reference.

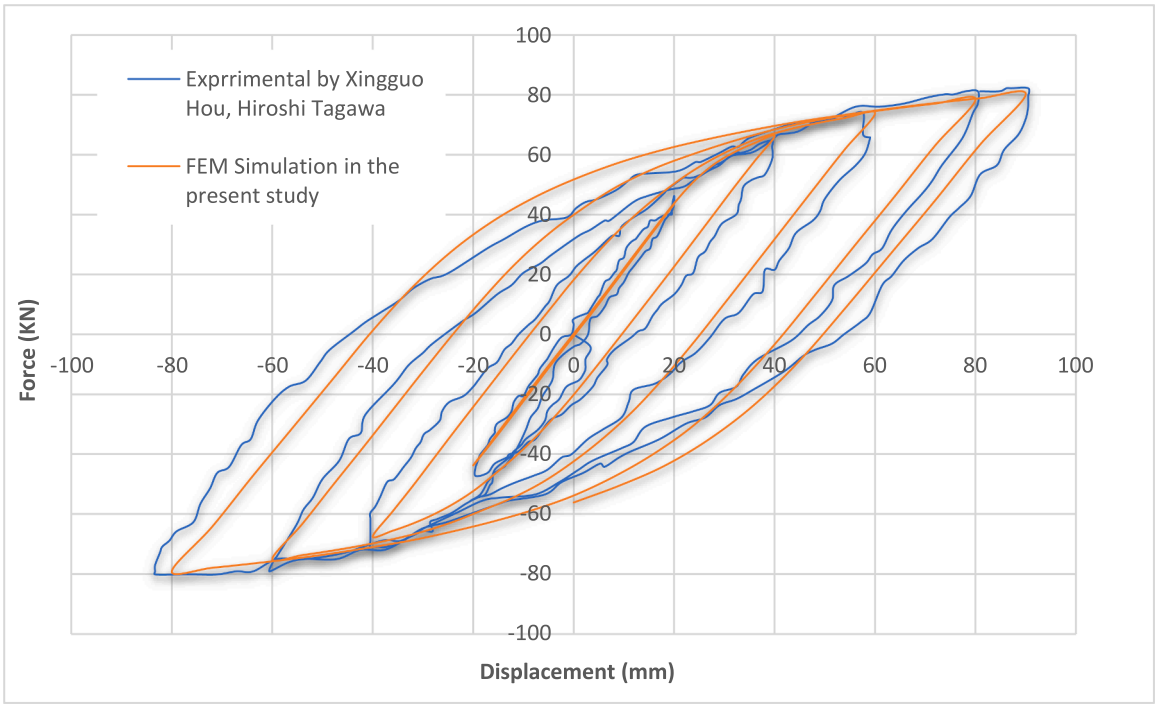

Fig. 26. Comparison between experimental test results by Hou and Tagawa [7] and FEM analysis results in this study.

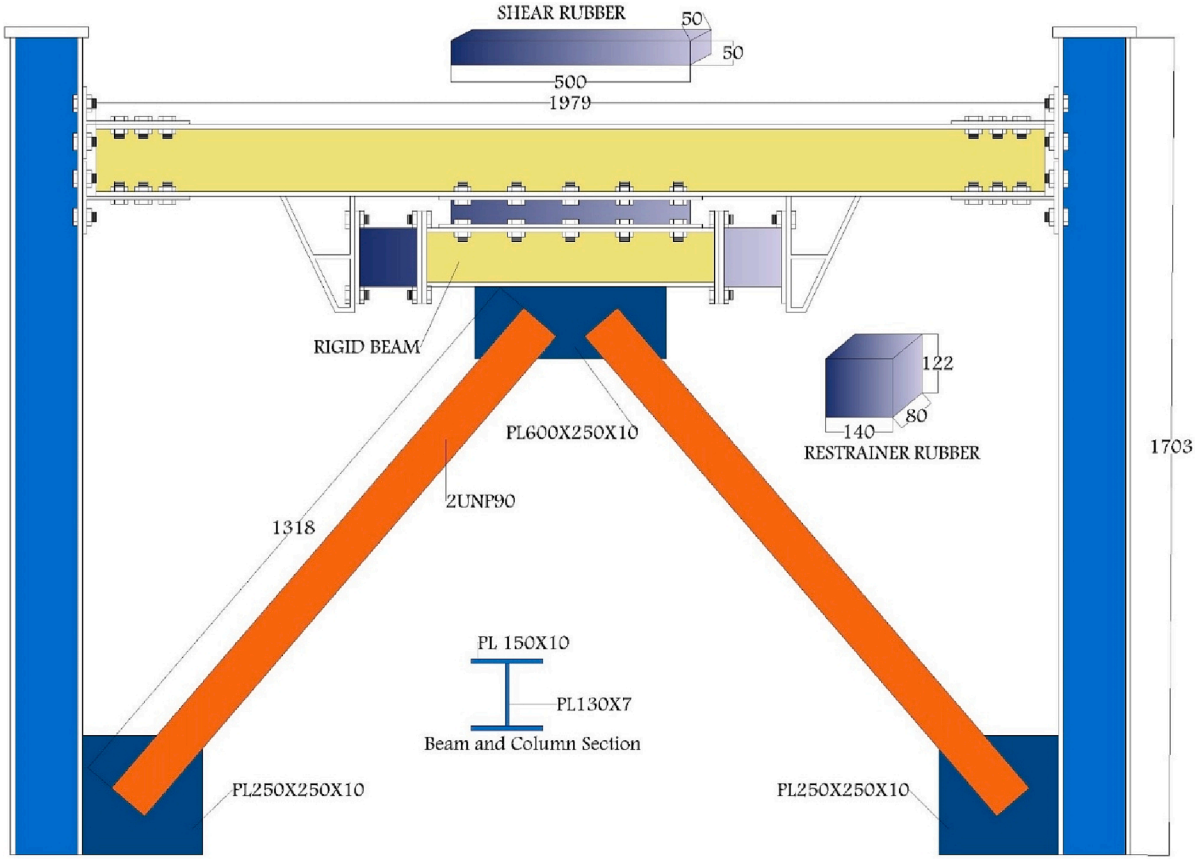

Fig. 27. Steel frame equipped with HRDR device.

The table illustrates that vulcanized rubbers have been tested within a range of 150% to 1000% elongations, exhibiting shear stress values ranging from 3 MPa to 29 MPa for elongations of 100% to 1000%, respectively.

These consistent results further support the conclusion that the rubber material can effectively withstand high deformations while

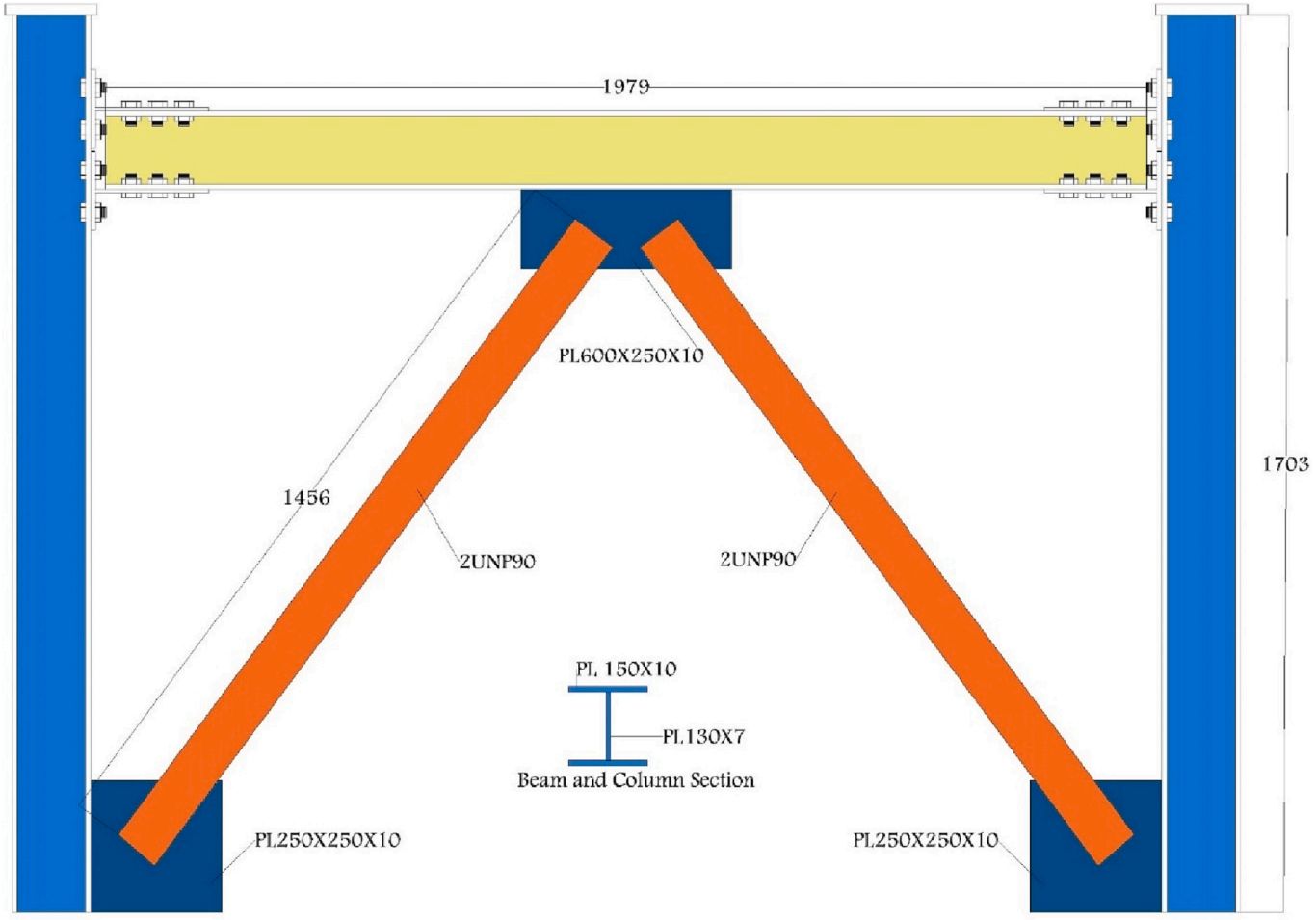

Fig. 28. Steel frame with Chevron brace (benchmark).

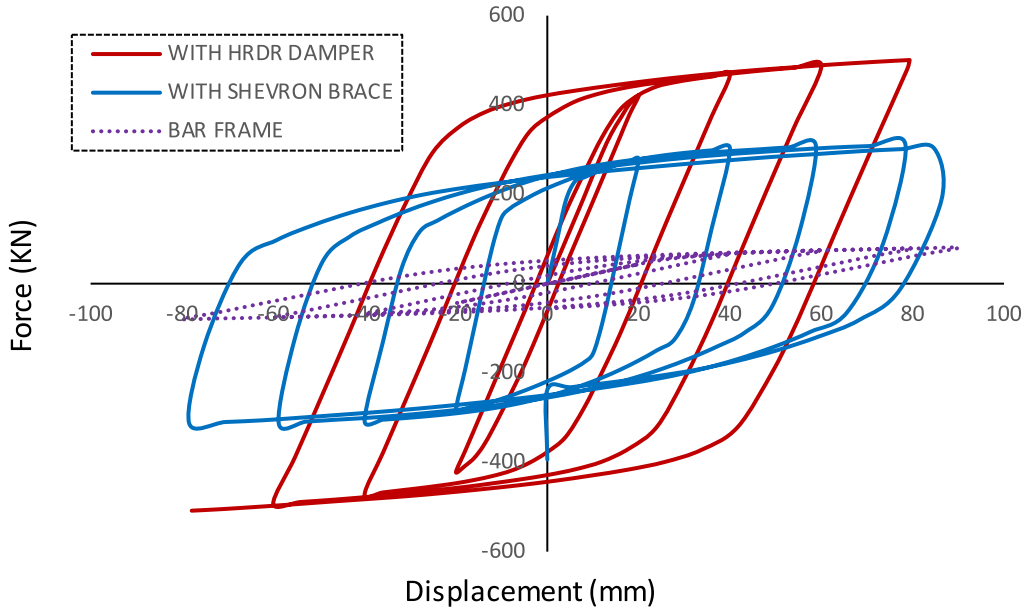

Fig. 29. Hysteresis results for steel frame furnished with HRDR device and steel frame with chevron and Bar Frame.

maintaining its integrity and vulcanization bonding with steel plates.

Fig. 23 is showing the stress contour for the rubber at maximum deformation of HRDR device corresponding to 150% of rubber thickness strain without implementing two rubber restrainers in the sides. As it can be seen in this figure, as expected the maximum stress is appeared in the contact between rubber and bottom steel plate which is around 3.4

Table 20
Summary of results for dissipated energy and maximum reaction force.

Frame	Energy dissipated (Mj)					Max Reaction Force (KN)				
	Cycle 1	Cycle 2	Cycle 3	Cycle 4	Total	Cycle 1	Cycle 2	Cycle 3	Cycle 4	Average
With HRDR System	3.29	34.027	70.99	178.94	287.24	420	468	488	500	469
With Chevron Brace	13.09	32.19	49.39	98.83	193.50	310	305.6	301.25	297.36	300

MPa. This is less than shear stress which has been experimentally tested for double shear rubber cylindrical specimen and it is indicating that vulcanised rubber is fully attached to the steel plate and fully function during applied deformation without any debonding and delamination.

It is worthy to highlight that implementing restrainer components in the proposed design for HRDR is limiting the movement of the rigid beam and preventing experience of any large deformation by shear rubber. Therefore, the maximum stress of the shear rubber in the HRDR device will never even reach to 3.4 MPa due to action of rubber restrainers which will prevent any damages to the vulcanised rubber.

6. Numerical verification of steel frame

In this research, a simple steel frame has been considered to implement the proposed Hybrid Rubber Damper Restrainer (HRDR) device to assess its effect on response of steel frame under cyclic loads. Fig. 24 shows the considered steel frame which experimentally tested by Hou and Tagawa [40] under cyclic loading. The column and beam sections were H-150 × 150 × 7 × 10 (steel grade: SN400B) which connected with bolted T-stubs cut from H-300 × 150 × 6.5 × 9 (SS400). Only the T-stubs exhibited plastic deformation during tests. Therefore, in this section, it is tried to verify simulation of steel frame using finite element method via experimental test results. Since only steel material has been used in this mode, the constitutive model is described as elastoplastic material and the main parameters regarding yield stress and plastic strain are listed in Table 19. The modulus of elasticity (E) and Poisson's ratio (ν) of the steel material are taken as 210GPa and 0.3, respectively. Also, the yield strength (σ_y) of steel material is taken as 300 MPa.

The reduced integration linear hexahedral solid element with eight-node and three degree of freedom (C3D8R) under hourglass control is used for simulation of steel parts in finite element modeling. Tie constraints are defined for the contact interface between column/beam and stiffener plate and hard contact has been used to model interaction between bolts and the body of other steel sections.

Various types of loading history have been implemented in the tests to evaluate the deformation characteristics of the structural members. A cyclic displacement-control loading protocol was adopted according to ASTM as shown in Fig. 25 and the load was laterally applied to the frames until yielding has been observed.

The comparison between the experimental and numerical results is presented in Fig. 26. The results proved that the numerical result is in a very good agreement with those of the experimental tests. Therefore, the FEM model of the considered steel frame has been validated to be used for further study in this research work.

7. Application of the developed hybrid rubber damper restrainer (HRDR) device in the steel frame

In order to assess performance of the developed HRDR device, it is implemented in a steel frame and subjected to cyclic loading as well as the earthquake excitation and then, the response of the steel frames under applied loads were investigated by comparing to the benchmark frame.

7.1. Modeling of steel frame equipped with the HRDR device

The proposed HRDR devices implemented in the steel frame which described and validated in the previous section (Fig. 27). The chevron bracing system with box section and dimension of 90 × 90 × 4 mm is used to install the HRDR in the frame which is connected to the base of the column by a plate with dimension of 250 × 250 × 10 mm and also connected to the center of rigid beam of HRDR by a plate with dimension of 600 × 250 × 10 mm.

Also, as shown in Fig. 28, the steel frame with chevron brace is considered with the same specifications as described before to use as a benchmark and subjected to the same cycle load protocol. The dimensions of the modeled frames and its details are shown in Figs. 27 and 28.

7.2. Performance of the steel frame with HRDR under cyclic load

The hysteresis results of the frame with HRDR and Chevron braced frame and bar frame are shown in Fig. 29 and Table 20. As can be seen in the results, equipping the steel frame with the HRDR resulted in higher force resistant capacity and limited displacement of the device. Therefore, the maximum damping force from 310 kN in the steel frame with chevron bracing is increased to the 500 kN in the frame with HRDR device which shows 61% increase in the load-bearing capacity of the frame by employing the developed HRDR device.

Table 20 shows the results of energy absorption in each loading cycle as well as the maximum support reaction of frames equipped with the HRDR system and Chevron bracing system. As can be seen, the amount of energy absorption per cycle in the frame equipped with the HRDR system is gradually increasing in each cycle to reach a total of 100% increase compared to the frame equipped with the Chevron bracing system.

As for the maximum reaction force, the amount of tolerable force in the frame equipped with the HRDR system increases in each cycle and finally reaches to the 500 kN, while the reaction force has a decreasing trend in the frame of the Chevron bracing and eventually it reaches to 297 KN.

In general, the results proved the effectiveness and ability of the developed HRDR device to endure high damping force and absorb high vibration energy. Also, based on the obtained results (Fig. 30-b), the bracing sections in the frames with Chevron bracing buckled due to the compressive force. The occurrence of buckling causes a sudden decrease in the load-bearing capacity and strength of the member. However, in the proposed system, as shown in Fig. 30-c, the proposed device prevents buckling of the bracing members.

The plastic analysis has been conducted to evaluate failure mode of each considered steel frame and the equivalent plastic strain for frames presented in Fig. 31.

Fig. 31-a shows the final stage deformation of the bare frame, which failed at the T-stub connection at joint A and subsequently at joint B (as marked in the figure) based on high equivalent plastic strain as 0.49 at the joint zone. Therefore, as it was expected, since it is moment resistant frame, the first failure and yielding strain is appeared in the joints due to high resistant against applied lateral load. However, the column members and beam member remained as elastic.

The failure mode of frame with Chevron bracing has been depicted in Fig. 31-b. As it can be seen in this figure, the maximum equivalent plastic strain about 1.87 is appeared at the middle part of bracing member with high deformation and yielding. Also, a part of the T-stub connection also experienced of some yielding around bolt and edge

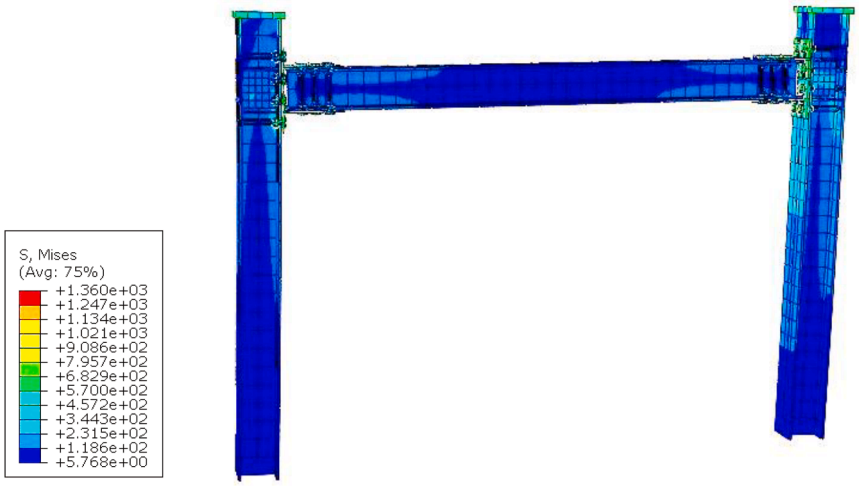

(a) Moment resistant steel frame (Bare frame)

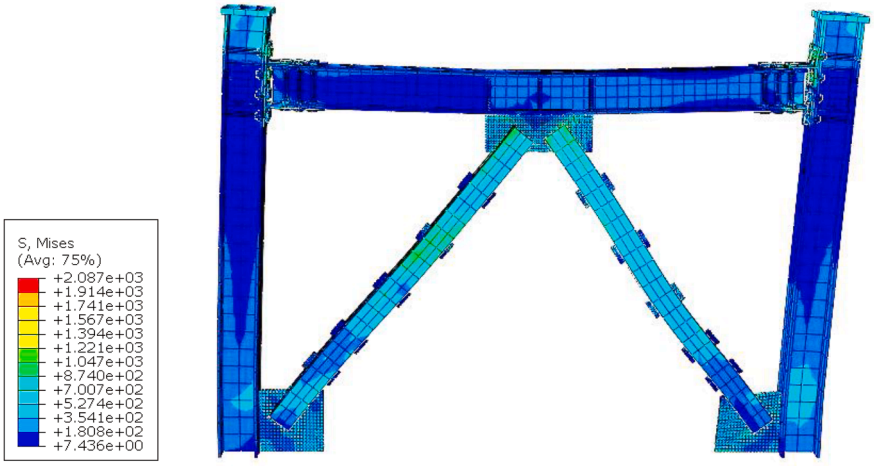

(b) Steel frame with chevron brace

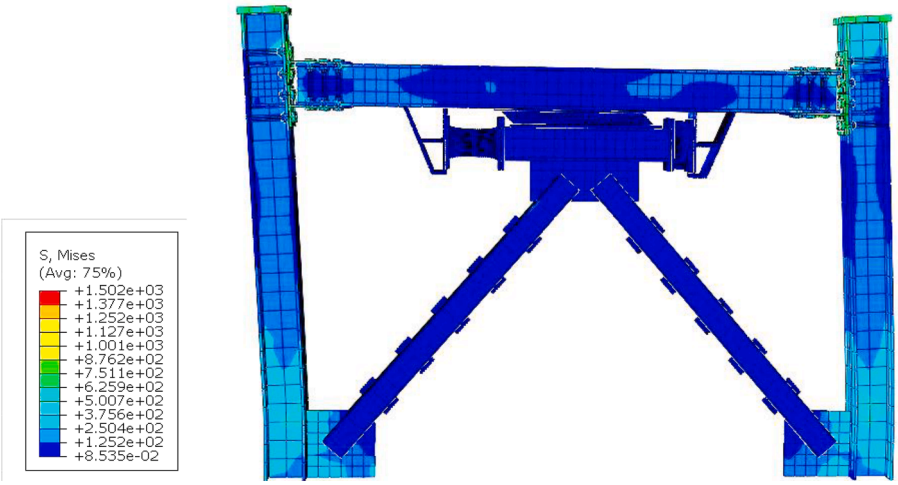

(c)Steel frame utilized with developed HRDR device

Fig. 30. Maximum stress in the considered frames under cyclic load.

flange due to applied load.

The plastic strain for the frame with DRDR at the last stage of deformation has been presented in Fig. 31-c. As it can be seen in this figure maximum equivalent plastic strain of 0.0438 has been observed in the join connections which is almost 91% less than bare frame and 96% less than frame with Chevron baring. While all other members include of columns, beams and Chevron bracings are totally in elastic stage. These results indicating the effectiveness of HRDR device to dissipate vibration effect on structure by noticeable reducing the plastic strain in the frame due to applied loads and prevent of any early failure mechanism in the structure.

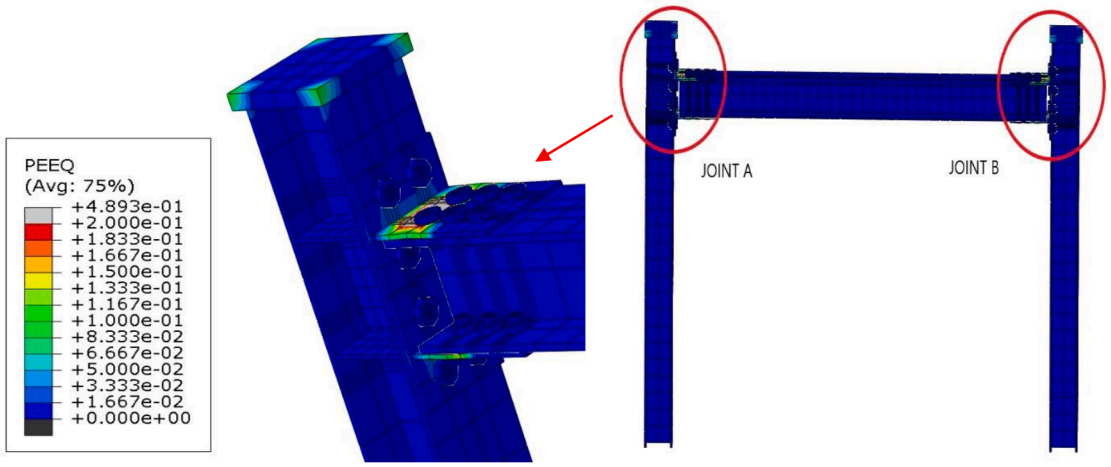

(a): The equivalent plastic strain for Steel bare frame

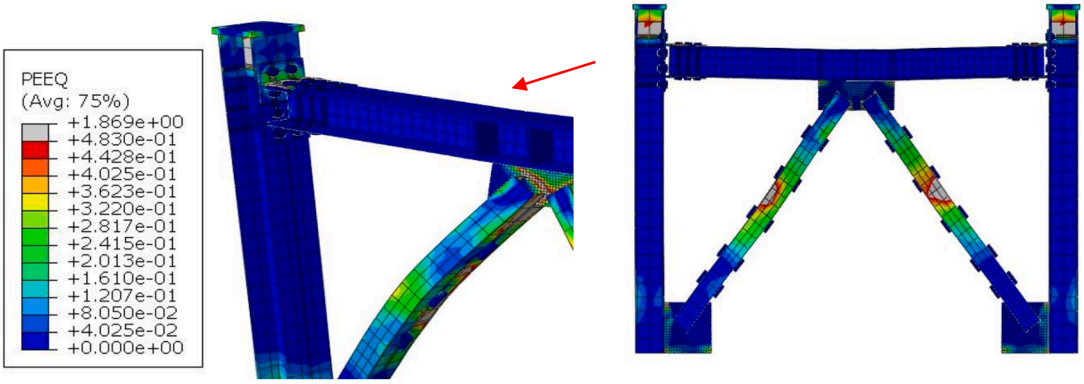

(b): The equivalent plastic strain for Steel frame with chevron bracing

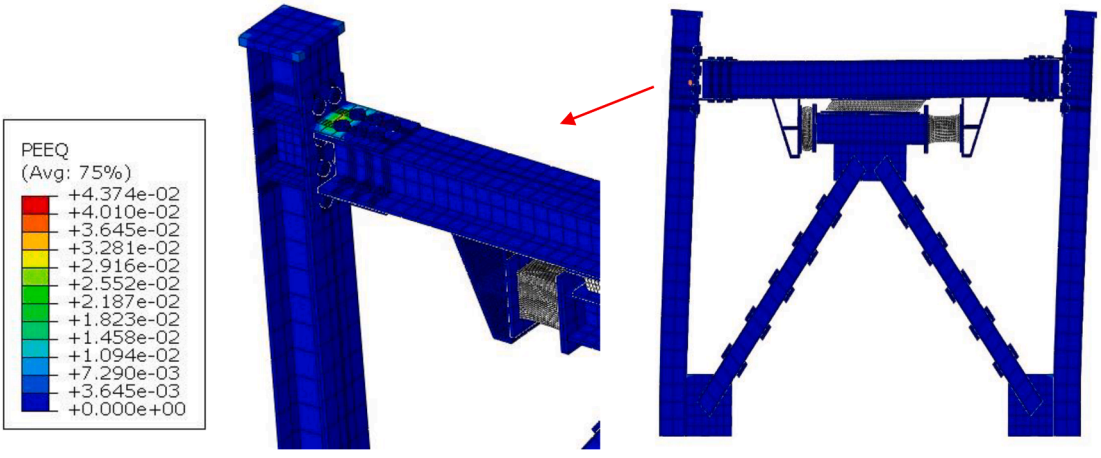

(c): The equivalent plastic strain for Steel frame with HRDR damper

Fig. 31. The equivalent plastic strain for considered frames and obtained yield modes.

7.3. Performance of the steel frame with rotational friction damper and HRDR device under earthquake excitation

To assess the performance of the proposed HRDR system, three following considered frames were considered and subjected to the El Centro earthquake record (USA-194):

1) The moment resistant steel frame (MRSF) (Bare Frame)

2) The moment resistant steel frame with hybrid rubber damper-restrainer (HRDR) device

3) The moment resistant steel frame with Rotational Friction Damper (RFDs) [41].

The time history analysis results in terms of time history

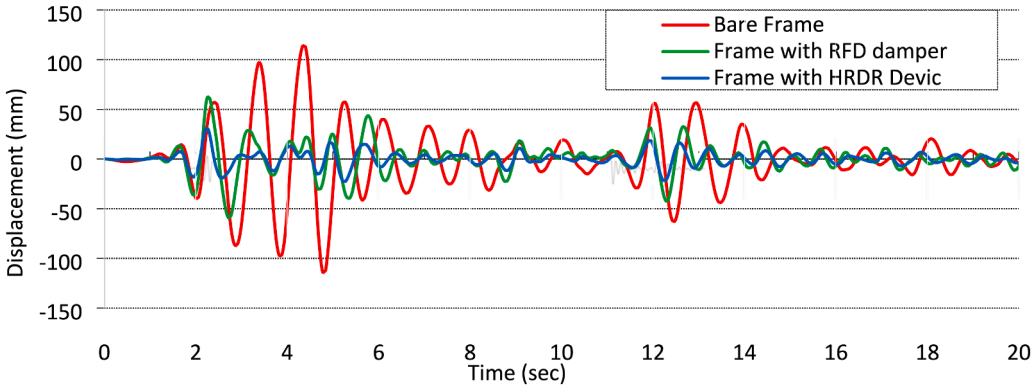

Fig. 32. Time history response of considered steel frames under applied El Centro earthquake.

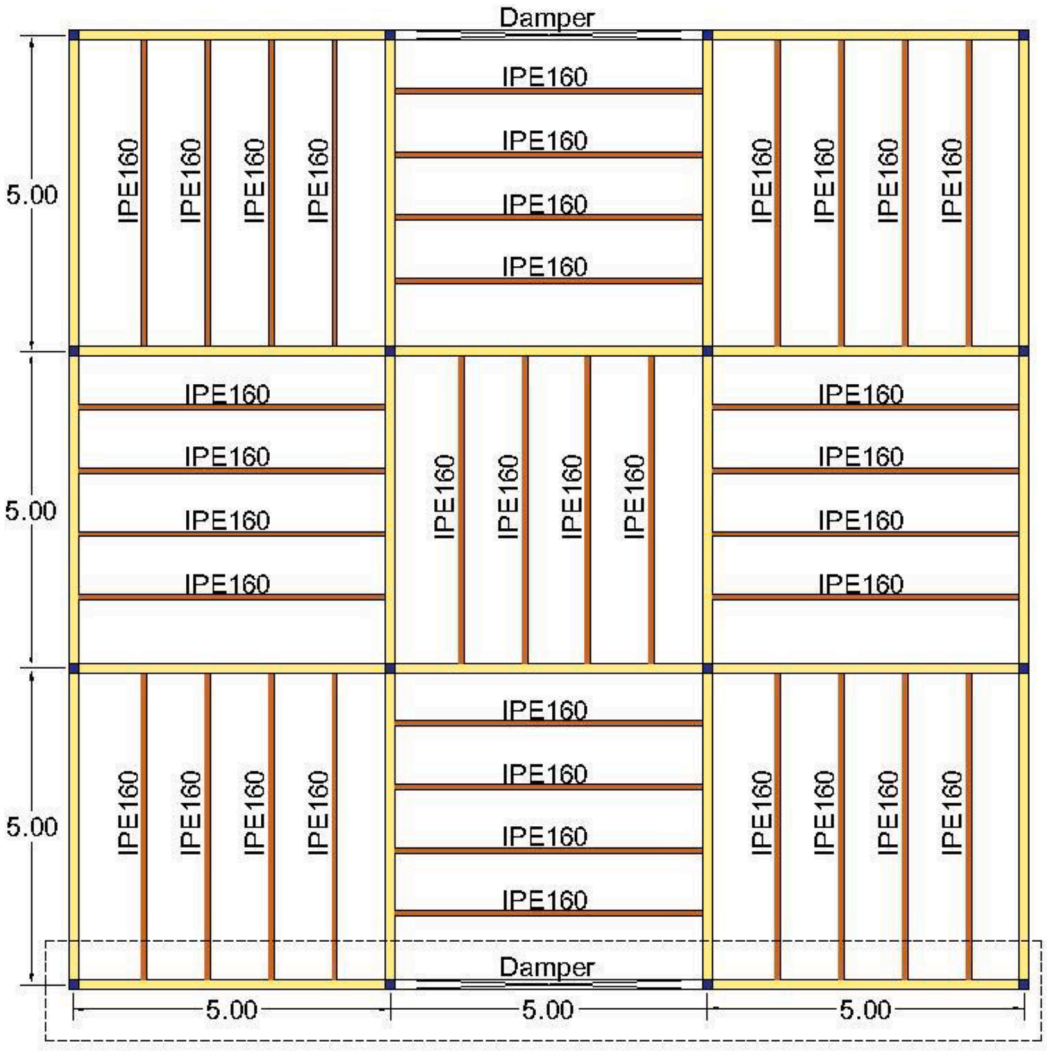

(a) Plan view

Fig. 33. Plan and elevation of an 8-story steel structure.

displacement for the considered frames are shown in Fig. 32.

As it can be seen in this figure, seismic response of structure has been reduced by implementing both damper devices into the frame under El Centro Earthquake. However, the results indicated that utilizing of HRDR device in the frame is more effective to reduce structural movement from 116 mm for bare frame and 60 mm for frame furnished with

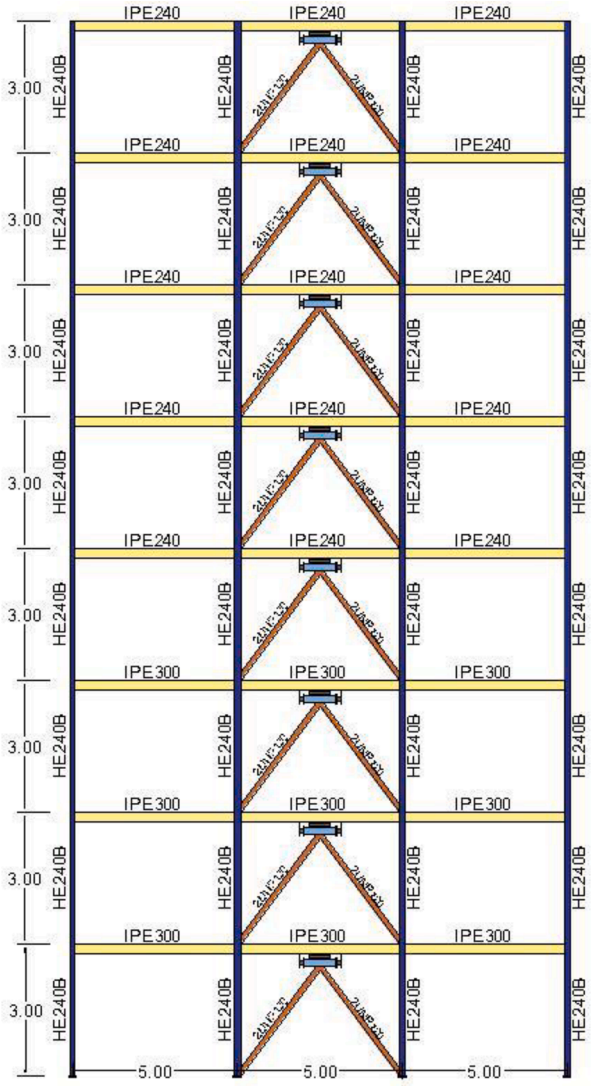

(b) Elevation view

Fig. 33. (*continued*).

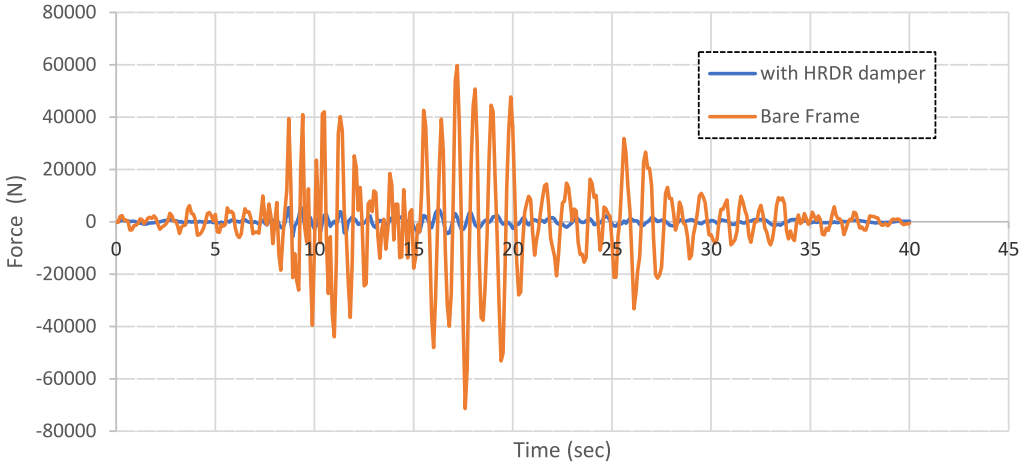

Fig. 34. Time-History of Base shear.

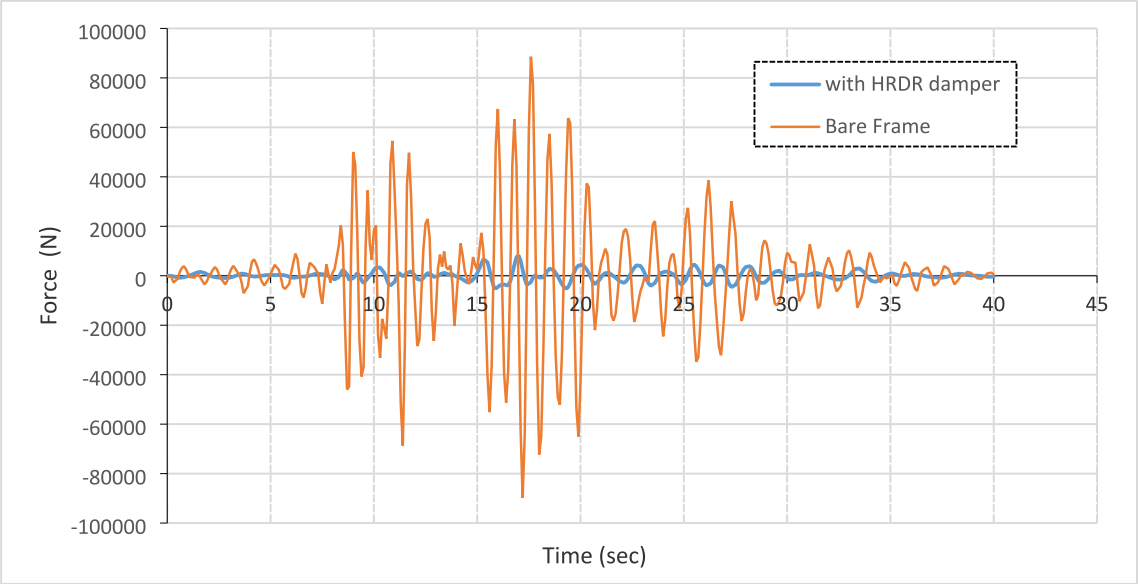

Fig. 35. Time-History of Axial forces in the Column C5.

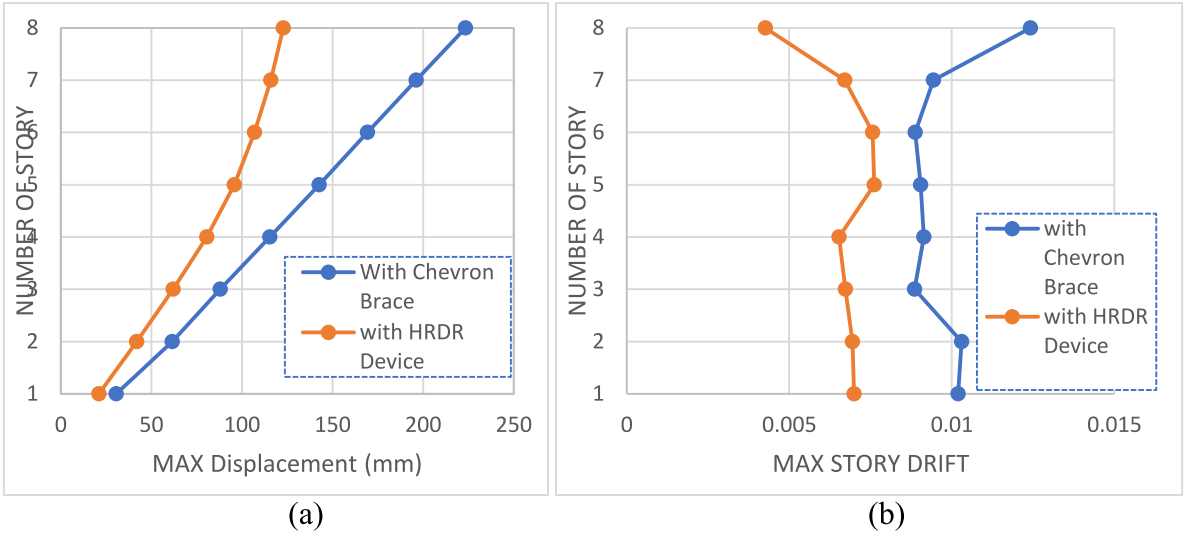

Fig. 36. Displacement response (a) and The inter-story drifts (b) of the structure with and without dampers under El Centro earthquake.

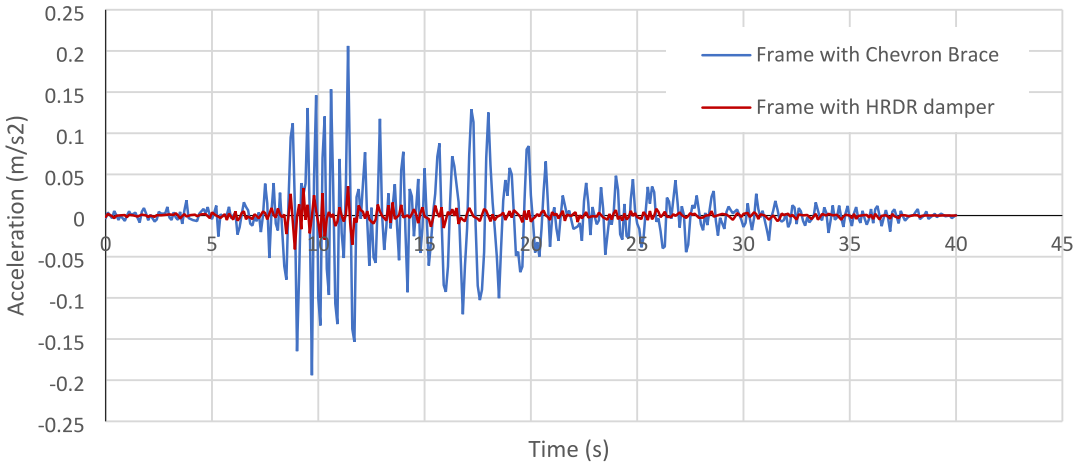

Fig. 37. Acceleration responses of the first floor under El Centro earthquake.

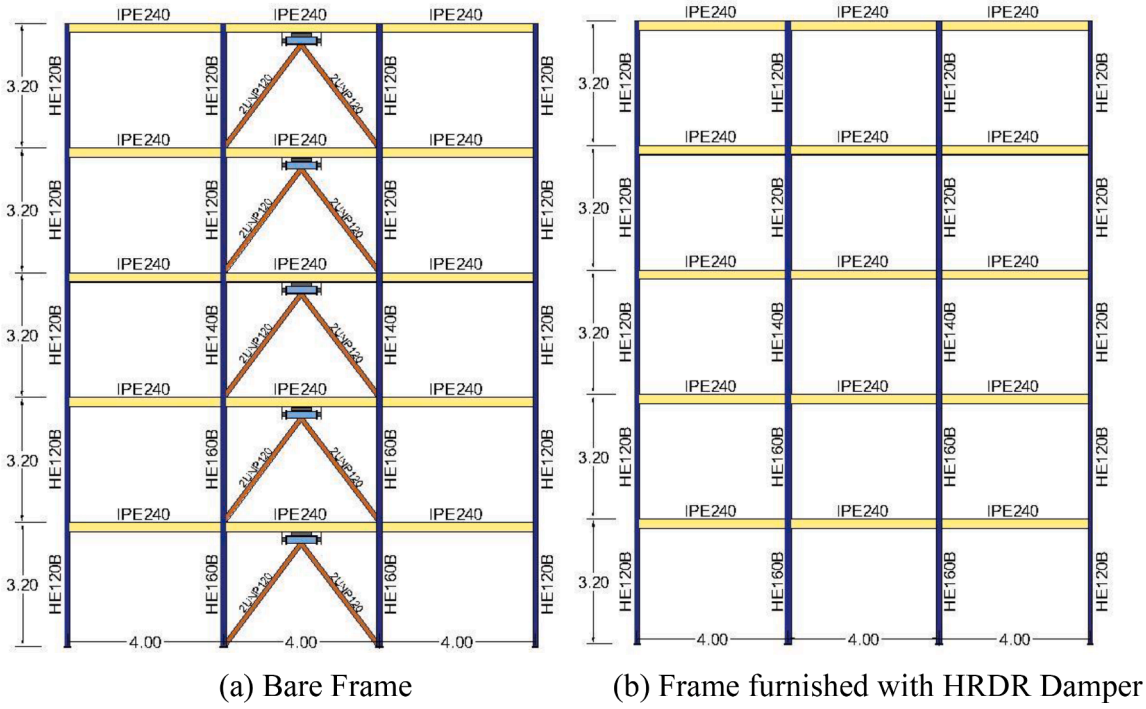

Fig. 38. Geometry and section properties of five-story steel framed model.

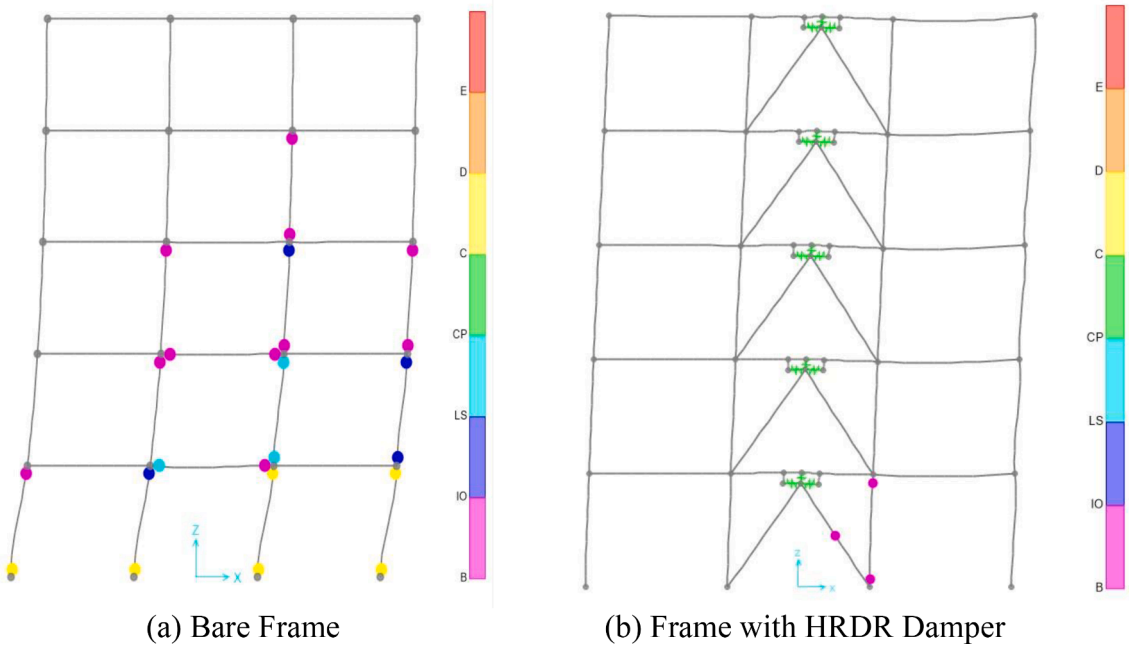

Fig. 39. Location of plastic hinge occurrence in the bare frame and also frame furnished with HRDR.

RFD damper device to 31.7 mm which is indicating 72% and 47% reduction respectively in structural displacement under earthquake excitation. Therefore, these results, proving high effectiveness of developed HRDR device to diminish effect of vibration on structure in comparison to the other types of damper devices such as Rotational Friction Damper.

8. Application of HRDR device in 8-story steel moment frame with HRDR dampers and chevron bracing system

The 8-story prototype residential building considered in this study has four perimeter lateral-load resisting frames in the longitudinal direction (as shown in Fig. 33). The design focuses on one of the four perimeter frames. This frame has three bays with a width equal to 5.0 m. The height of all stories is 3 m, beams and columns are made of S275 steel grade. In order to evaluate the performance of the proposed damping system and also to compare the performance with the Chevron bracing system, the eight-story frame of the previous part was first equipped with a Chevron bracing system and then, by replacing the proposed damping system (HRDR) with a Chevron brace, it was modeled and nonlinear analysis has been conducted under the EL Centro earthquake record.

Table 21
The numbers of plastic hinges in structural section according to various performance levels.

Structure Type	Plastic Hinge Numbers According to Performance Levels											
	Beam				Column				Brace			
	<IO	IO-LS	LS-CP	>CP	<IO	IO-LS	LS-CP	>CP	<IO	IO-LS	LS-CP	>CP
Bar Frame	3	0	1	0	6	3	2	9	\mathord{-} -	\mathord{-} \mathord{-}	\mathord{-} -	\mathord{-} -
Frame with HRDR Damper	0	0	0	0	2	0	0	0	1	0	0	0

Table 22
The maximum plastic hinge rotations in the bare frame and frame with HRDR device.

Structure Type	Maximum Plastic Hinge Rotation Values (rad)		
	Beam	Column	Brace
Bar Frame	0.037152	0.055942	\mathord{-} \mathord{-}
Frame with HRDR Damper	0	0.000909	0

For this purpose, the value of shear force on the ground floor as well as the axial force generated in the lower floor column and the maximum story drift and displacement are examined and the results are shown in the Figs. 34–36. The results show the acceptable performance of the proposed damping system (HRDR) in reducing the base shear force of the building and also reducing the axial force generated in the bracing column and about 30% reducing in story drift were obtained using ETABS.

The compression forces in the left column of the first floor were considered to evaluate effect of the damper. Changes in the axial force of the column under El-Centro ground motion are shown in Fig. 35. As can be observed, compared to the conventional bracing system, the axial forces of the column in the frame equipped with the damper, are remarkably reduced.

Fig. 36 show comparison of the displacement responses and story drift between the structures with chevron bracing and HRDR dampers under El-Centro earthquake excitations. It can be seen in these figures that the displacement and maximum story drift responses are noticeable reduced by implementing HRDR damper instead of Chevron bracing.

When HRDR dampers are installed in the structure, the maximum displacement response decreased from 223.2 mm to 122.8 mm by 44.9% under El-Centro excitation.

Fig. 37 shows comparison of the acceleration responses of the first floor between the structures with chevron braces and HRDR dampers under the El-Centro earthquake excitations. As shown in the graph, the utilization of HRDR damper in the frame instead of a bracing system resulted in a significant decrease in the maximum acceleration response for the first floor from 0.206 m/s^2 to 0.0356 m/s^2 under El Centro excitation. This improvement can be attributed to the implementation of HRDR dampers, which provide a structure with more flexibility (lower stiffness) and higher damping compared to a bracing system. Indeed, having a more flexible and higher damping system is beneficial for dissipating and mitigating structural damages caused by excessive movement.

So, based on present result, the developed earthquake energy dissipation system successfully diminished the seismic effect on the building seismic response in terms of forces in the structural member and displacements, which ensures the safety of structures in severe dynamic load excitation.

9. Application of HRDR in 5-story steel framed building

The finite element modeling of five story building is considered as depicted in Fig. 38. All dimensions and section details for the beams and columns are shown in the same figure. Steel ST37 grade was chosen for material and section properties of the beam and column members are showed in Fig. 38. The distribution dead and live loads on beams is 18 and 6 KN/m respectively.

First, the Nonlinear Static Analysis (PUSHOVER) carried out for structure without any damper device. After performing analysis, the plastic hinges are occurred in beam and column members as shown in Fig. 39 at the end step of loading.

So, the HRDR dampers were added to the middle bay in all stories of the building to evaluate the effect of HRDR dampers in capacity of structure as well as in inelastic response of the frame. Position of the damper elements in the frame model is portrayed and depicted in Fig. 38-b.

Location of plastic hinge occurrence in the bare frame and also frame furnished with HRDR is showed in Fig. 39 and summarized in Table 21.

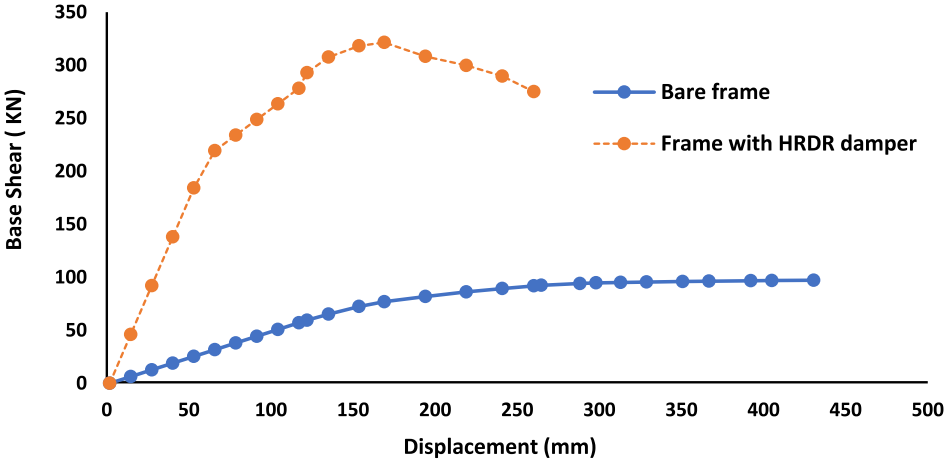

Fig. 40. Pushover curve for the bare frame and frame with HRDR Damper.

As it can be seen in the results, the total number of plastic hinges in the bare frame for all different performance levels of IO/LS/CP is reduced from 24 to 3 only (87% reduction) by utilizing HRDR dampers in the frame. The results showing that there is no plastic hinge on IO-LS performance level of structure equipped with HRDR device and structure able to continue its operation without experiencing any seismic damage. Therefore, HRDR device is successfully abled to dissipate seismic effect on structure and increase stability and safety of the structure.

The maximum plastic hinge rotations in the bare frame and frame with HRDR device are presented in Table 22. As it can be seen in this result, there is no any plastic hinge rotation in the frame furnished with HRDR and implementing of this device in the structures is resulted to reduce plastic hinge rotation in the columns from 0.055942 rad to 0.000909 rad (only 2 plastic hinge in the column) with 98% reduction.

Fig. 40, shows pushover curve for the bare frame and frame furnished with HRDR device. It is obvious from this figure that the maximum horizontal displacement of the bare frame with 644 mm movement is restrained by HRDR device to 430 mm which indicating 33% reduction in lateral deformation. While the resistant force of the bare frame from 100 kN is noticeably increased to 335 kN by utilizing HRDR device which proving successful effect of HRDR device on performance of the structure to enhance its capacity by 250%.

10. Conclusions

In the present study, a new Hybrid Rubber Damper-Restrainer (HRDR) system is developed by utilizing the high damping rubber components at middle of steel beam and two hyper-elastic rubber restrainer components at both sides of the beam.

Performance of the proposed HRDR damper device is verified and investigated using the FEM analysis and following concluding remarks have been derived:

1) High energy absorption provided by the HRDR device up to about 1,870 KN.M, stiffness of 887 KN/mm and also equivalent damping of 10,700 (KN.s/mm).
2) The results showed that 95% of the stiffness of the HRDR device is due to the action of restraining rubber in the proposed system. Also, the storage modulus G_1 and the loss factor η augment with increase in the load frequency.
3) The stiffness and damping of the structures increased about 130% at low frequencies (0.25 and 0.5 Hz and 0.75 Hz) and about 220% at high frequencies (1 Hz).
4) Accordingly, the highest energy absorption was related to the applied displacement equivalent to 150% strain with loading frequency of 1 Hz.
5) The displacement response of considered prototype structure and story drift response is reduced around 43.5% and the acceleration response decreased by 82% when HRDR dampers are installed in the prototype structures instead on bracing system.
6) The results showed a reduction about 95% for the generated force in the column of frame equipped with the HRDR damper compared to the chevron brace.

Therefore, in overall, the results of this study proved the capability of developed HRDR device in mitigating the effect of applied vibration in the prototype structures and also restraining the movement of structures to protect them against catastrophic excitations. Based on the results of this study, it is recommended as a future study to conduct experimental tests to assess the performance of the installed HRDR in the frame structures. This would involve evaluating the response of steel or reinforced concrete (RC) frames equipped with the HRDR prototype device under lateral load or vibration excitations.

Declaration of Competing Interest

The authors declare that they have no known competing financial interests or personal relationships that could have appeared to influence the work reported in this paper.

References

[1] Tsai CS. Innovative design of viscoelastic dampers for seismic mitigation. Nucl Eng Des 1993;139(2):165–82.
[2] Mahmoodi P. Design and analysis of viscoelastic vibration dampers for structures. Proc INOVA73 World Innovative Week Conference. 1974.
[3] Hejazi F, Zabihi A, Jaafar MS. Development of elasto-plastic viscous damper finite element model for reinforced concrete frames. Soil Dyn Earthquake Eng 2014;65:284–93.
[4] Charney JD, Marshall FA. A hybrid passive control device for steel structures. J Constr Steel Res 2010;66:1278–86.
[5] David Koblar, Miha Boltezar, "Evaluation of the frequency-dependent Young's modulus and damping factor of rubber from experiment and their implementation in a," Experimental Techniques, vol. 40, no. doi: 10.1007/s40799-016-0027-7, p. 235–244, 2013.
[6] Hao D, Li D, Liao Y. A finite viscoelastic constitutive model for filled rubber-like materials. Int J Solids Struct 2015;64-65:232–45.
[7] Lion, Hoofer and, "Displacement-restraint bracing for seismic retrofit of steel moment frames," Journal of Constructional Steel Research, vol. 65, pp. 1096-1104, 2009.
[8] Shahzad M, Kamran A, Siddiqui MZ, Farhan M. Mechanical characterization and FE modelling of a hyperelastic material. Mater Res 2015;18(5):918–24.
[9] Jieying Zhi, Shenping Wang · Mengjie Zhang, "Numerical analysis of the dependence of rubber hysteresis loss and heat generation on temperature and frequency," Mech Time-Depend Mater, 2018.
[10] Farzad Hejazi, Mohammad Dalili Shoaei, Mohd Saleh Jaafar,and Raizal Saiful Bin Muhammad Rashid, Effect of viscous dampers on yielding mechanisms of RC structures during earthquake, Earthquakes Struct, vol. 8, pp. 1499-1528, 2015.
[11] Bae J, Karavasilis TL. Seismic design and assessment of steel frames with visco-plastic dampers. Int J Earthquake and Impact Eng 2018;2(4):282.
[12] Zhao G, Pan P, Qian J, Lin J, Experimental study of viscoelastic dampers subjected to large deformation, J Build Struct, 2012.
[13] Hejazi F, Shoaei MD, Tousi A, Jaafar MS. Analytical model for viscous wall dampers. Comput Aided Civ Inf Eng 2016;31(5):381–99.
[14] Jabbareh Asl M, M. Rahman M, Karbakhsh A. Numerical analysis of seismic elastomeric isolation bearing in the base-isolated buildings. J Earthquake Res 2014;03(01):1–4.
[15] Xu ZD, Wang DX, Shi CF. Model, tests and application design for viscoelastic dampers. J Vib Control 2011;17(9):1359–70.
[16] Ansarifar MA, Zhang J, Baker J, Bell A, Ellis RJ. Bonding properties of rubber to steel, aluminium and nylon 6, 6. Int J Adhes Adhes 2001;21(5):369–80.
[17] American Society for Testing and Material, Standard Test Methods for Vulcanized Rubber and Thermoplastic Elastomers-Tension, 2018.
[18] ISO, 37, Rubber, vulcanized or thermoplastic — Determination of tensile stress-strain properties, 2017.
[19] ASTM, D595-85, Standard Specification for Tetrasodium Pyrophosphate, 1997.
[20] ISO, 7743, Rubber, vulcanized or thermoplastic — Determination of compression stress-strain properties, 2017.
[21] ASTM D945-22, Standard Test Methods for Rubber Properties in Compression or Shear, 2022.
[22] Shitole RR, Chavan US, Dolse S. A review on methodology of material characterization and finite element modelling of rubber-like materials. J Eng 2018:06–10.
[23] Yeoh, Oh, Hyperelastic material models for finite element analysis of rubber, J Natural Rubber Res, vol. 12(3), p. 142, 1997.
[24] Ogden RW. Large deformation isotropic elasticity–on the correlation of theory and experiment for incompressible rubberlike solids. Proceedings of the Royal Society of London. A. Mathematical and Physical Sciences 1972;326(1567):565–84.
[25] Sun JWD, Liu S, Zhang X. Damping Characteristics of Viscoelastic Damping. Mathematical and Computational Applications 2017.
[26] Habieb AB, Milani G, Quaglini V, Milani F. Relaxation test and numerical modeling of rubber for seismic base isolation. AIP 2019.
[27] Saedniya M, Talaeitaba SB. Numerical modeling of elastomeric seismic isolators for determining force–displacement curve from cyclic loading. Int J Adv Struct Eng 2019;11(3):361–76.
[28] Chen Y, Che C, Ma Q, Jiang Huanjun, ZhiweiWan. Study on mechanical properties of high damping viscoelastic dampers. Adv Struct Eng 2019;22(14):2925–36.
[29] Xijin Feng, Zhichao Li, Yintao Wei, Yalong Chen, Michael Kaliske, Christoph Zopf and Ronny Behnke, "A novel method for constitutive characterization of the mechanical properties of uncured rubber," Journal of Elastomers & Plastics, pp. 1-12, 2015.
[30] Xu ZD. Earthquake mitigation study on viscoelastic dampers for reinforced concrete structures. J Vib Control 2007;13(1):29–45.
[31] T. Documents, "MIKI PULLEY General Properties of Vulcanized Rubber," 2022.
[32] Janusz Datta PK. Effect of high loading of titanium dioxide particles on the morphology, mechanical and thermo–mechanical properties of the natural rubber–based composites. Iran Polym J 2016;25:1021–35.

[33] Budiman BA, Sambegoro PL, Rahardian S, Ilhamsyah R, Firmansyah R, Juangsa FB, et al. Prediction of the remaining service lifetime of inflatable rubber dam with deep hole damage. Indonesian J Sci Technol 2020;5(3):366–81.
[34] Zhou Y, Li D, Shi F, Luo W, Deng X. Experimental study on mechanical properties of the hybrid lead viscoelastic damper. Eng Struct 2021;246:113073.
[35] Li H, Xie Y, Gu Y, Tian S, Yuan W, DesRoches R. Shake table tests of highway bridges installed with unbonded steel mesh reinforced rubber bearings. Eng Struct 2020;206:110124.
[36] Pawar VS, Pant RS, Guruprasad PJ. Experimental and numerical studies on the effect of elongation rate and temperature on the mechanical behaviour of high strength NBR. Plast, Rubber Compos 2019;48(7):281–92.
[37] Kumar S. (2014). Influence of Interrupted Vulcanization on the Rubber to Metal Bonding Strength.
[38] Nguyen XD, Guizani L. Analytical and numerical investigation of natural rubber bearings incorporating U-shaped dampers behaviour for seismic isolation. Eng Struct 2021;243:112647.
[39] Fujita T. Seismic isolation rubber bearings for nuclear facilities. Nucl Eng Des 1991; 127(3):379–91.
[40] Hou X, Tagawa H. Displacement-restraint bracing for seismic retrofit of steel moment frames. J Constr Steel Res 2009;65(5):1096–104.
[41] Liao W-I, Mualla I, Loh C-H. Shaking-table test of a friction-damped frame structure. The structural design of tall and special buildings. 2004. p. 45–54.